State of Health estimation of battery systems

Carl Spångberg

LUND
UNIVERSITY

Department of Automatic Control

MSc Thesis
TFRT-6214
ISSN 0280-5316

Department of Automatic Control
Lund University
Box 118
SE-221 00 LUND
Sweden

Printed in Sweden by Tryckeriet i E-huset
Lund 2023

Abstract

This study focuses on estimating the state of health (SoH) of a lithium iron phosphate (LFP) battery system, which is crucial for assessing the value and lifespan of new or used batteries in energy storage, grid support, and electric vehicle applications. A proposed method for determining SoH based on comparing useful and nominal useful capacities in Ah and Wh, as well as total and nominal capacity, has been presented. To validate the method, 200 charging and discharging cycles over five months were performed. Three models were developed to track battery behavior and one model to simulate degradation. An extended Kalman filter has been used in the model to estimate the battery's non-linear parameters and filter the noisy measurements. The models revealed that while estimating capacity using Coulomb and Watt counting proved difficult for the battery system that has been used, weighted least squares and recursive weighted least squares methods showed promise for determining current capacity. Furthermore, an attempt to estimate the battery's equivalent series resistance was performed, but no conclusion could be drawn due to limited knowledge of battery parameters. The findings highlight the challenges of modeling and estimating the SoH of used batteries and suggest the need for more targeted experimentation to improve battery modeling and estimation accuracy.

Acknowledgements

I would like to thank everyone for making this thesis possible. Adam Madsen and Magnus Dam-Hendriksen for helping me make the battery work and fixing problems. The people at Nerve Smart Systems with troubleshooting the battery. My supervisors at DTU are Zoltan Mark Pinter, Dimitrios Papageorgiou, and Chunyang Zhao. My supervisor at LTH, Richard Pates. Felix Bille to help with the script for data processing. Lastly, I would like to thank William Marnfeldt and Enrico Corato.

Preface

This Master's Thesis was performed at the Technical University of Denmark under the supervision of Lund University on the topic of State of Health (SoH) estimation of battery systems.

It was performed from the start of November 2022 until the start of April 2023.

The purpose of this thesis is to figure out a way to estimate the state of health of an LFP battery system to apply it to the battery system in the lab, and to see what the SoH of the battery system is.

The battery testing generates a lot of data for the charging and discharging performance of LFP battery cells. The results will be public and allow for further research on LFP cells.

List of Figures

List of Tables

List of Abbreviations

Abbreviation	Meaning
AC	Alternating current
BMS	Battery management system
CC	Constant current
CCCV	Constant current constant voltage
C-rate	Current rate
DC	Direct current
DoD	Depth of discharge
DV	Differential voltage
EC	Equivalent circuit
ECh	Electro-chemical
EKF	Extended Kalman filter
EoL	End of life
EV	Electrical vehicles
KF	Kalman Filter
LFP	Lithium iron phosphate
RLS	Recursive least squares
RSS	Residual sum of squares
R_0	Equivalent series resistance
SoC	State of charge
SoH	State of health
TSS	Total sum of squares
V_{oc}	Open circuit voltage
WLS	Weighted least squares

List of Symbols

Symbol	Unit	Definition
V_{oc}	V	Open circuit voltage
i	A	Current in the system
R_0	Ω	equivalent series resistance of the battery
R_1	Ω	Resistance in the $resistor_1$ and $capacitor_1$ branch
R_2	Ω	Resistance in the $resistor_2$ and $capacitor_2$ branch
V_0	V	Voltage over the equivalent series resistance
V_1	V	Voltage over $resistor_1$ and $capacitor_1$ branch
V_2	V	Voltage over $resistor_2$ and $capacitor_2$ branch
C_1	F	Capacitance in the $resistor_1$ and $capacitor_1$ branch
C_2	F	Capacitance in the $resistor_2$ and $capacitor_2$ branch
V_{term}	V	Terminal voltage of a battery cell
τ	s	time constant of the system
T	$°C$	Temperature
SoC	%	State of charge
SoH	%	State of health
Q_{Ah}	Ah	Capacity of the battery in Ah
$Q_{nom,Ah}$	Ah	nominal capacity of the battery in Ah
$Q_{nom,Wh}$	Wh	nominal capacity of the battery in Wh
$Q_{u,Ah}$	Ah	Useful capacity of the battery in Ah
$Q_{u,nom,Ah}$	Ah	Useful nominal capacity of the battery in Ah
Q_{Wh}	Wh	Capacity of the battery in Wh
$Q_{u,Wh}$	Wh	Useful capacity of the battery in Wh
$\hat{Q}_{u,Ah}$	Ah	Estimated useful capacity in Ah
$\hat{Q}_{u,Wh}$	Wh	Estimated useful capacity in Wh
η	%	Efficiency

Contents

1

Introduction

Knowing the state of health (SoH) is necessary for safe and reliable operations of batteries. In addition, the SoH can help determine the viability of the battery and what purposes it can be used for. Using a battery and knowing its SoH might also help in problems related to renewable energy production, such as stabilizing the electrical grid and increasing the reliability of charging an EV. The importance of determining the SoH of a battery system to acquire a battery will be highlighted. The chapter will end with the goal of the thesis and the content of the coming chapters.

Background

It is essential to know a battery's State of Health (SoH), i.e., how much the battery has degraded from its nominal values. The SoH indicates how well the battery will perform and how long it can be used. Unfortunately, there is not a clear consensus on the definition of SoH. Therefore, the SoH will be discussed in more detail in Chapter 2. Determining SoH is essential to determine if the batteries are worth the investment and how long they can be used. However, knowledge of the number of cycles, current capacity, and initial technical specification might be unknown when acquiring a battery that has been used, for example, an old EV battery.

The use of batteries in different applications has increased over the years [Bloch et al., n.d.]. The climate crisis and the rising cost of electricity, as seen in Figure 1.1, have created a larger incitement to install more renewable energy, such as solar and wind-power [UN, n.d.]. The hope of producing and using energy with a lower carbon footprint has entered sectors such as the energy and transportation sectors, to name a few. Cheaper and lower carbon footprint electricity generation increases electric vehicle (EV) viability since charging EVs becomes cheaper and more sustainable. However, the increased use of renewable energy is not without its problems [Trafikanalys, n.d.]. Renewable energy is an intermittent source of energy, which can cause problems with the current electrical grid. In addition, intermittent energy sources are not dependable, meaning that electricity production cannot be controlled. For example, wind and solar power are intermittent sources of energy because when the wind blows, and there is sunlight, it can not be controlled to produce electricity from a wind turbine and solar panel.

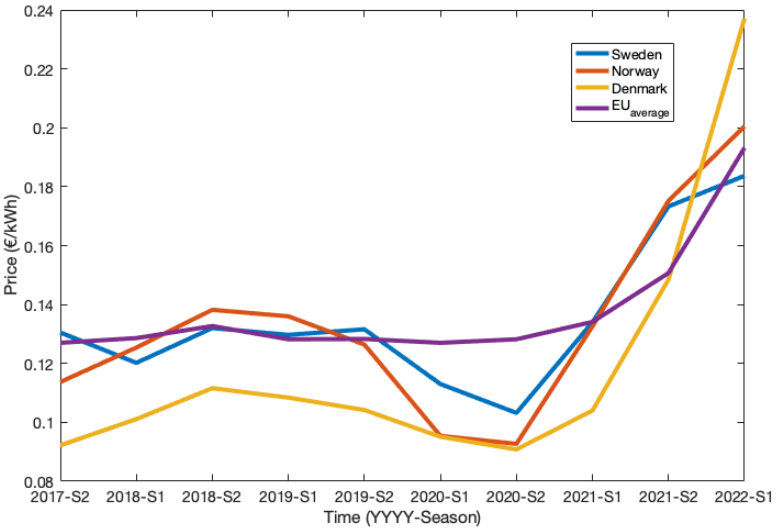

Figure 1.1 Illustrates a steady price for household consumers for years and a large price increase by a factor of two in recent years [Eurostat, n.d.].

Intermittent sources of energy can produce instabilities in the electrical grid. The instabilities can be caused by production not meeting the electricity demand. The difference between production and demand can affect the grid frequency. Changes in the grid frequency can cause problems in the electrical grid with blackouts or machine tripping [entsoe, n.d.].

With renewable energy in consideration, changes in the electrical grid frequency are partly due to the inertia problem [Pates and Mallada, 2018]. Wind power can produce direct current (DC) or alternating current (AC) (depending on the generator in the turbine). However, the electricity is transformed to DC and then transformed again to AC and supplied to the grid. The transformation of AC to DC and back to AC loses all the inertia that the wind turbine has in the spinning of the rotor blades, and therefore, wind turbines have more or less no contributing inertia. Solar power has no inherent inertia since it only produces DC. Some inverters can emulate inertia or compensate for changes to the grid [Denholm et al., 2020].

With less inertia, the frequency of the grid can become less stable. The lower stability is caused by changes in produced and consumed power affecting the change in frequency to a greater extent. Equation (1.1) shows the relationship between the inertia, power consumed and power generated.

$$\frac{df(t)}{dt} \propto \frac{1}{M}(p_g - p_c) \tag{1.1}$$

$\frac{df(t)}{dt}$	The change in grid frequency	
p_g	Power generated	[entsoe, n.d.]
p_c	Power consumed	
M	Total moment of inertia in the grid	

The larger M in the electrical grid is, the less changes in p_g and p_c affect the changes in grid frequency. Suppose M is close to zero. Then the effect that p_g and p_c have on the change in frequency gets amplified. The amplification occurs because M sets the time constant in the system. If (p_g - p_c) increases, the frequency decreases; when (p_g - p_c) decreases, the frequency increases. Hydropower is, to some extent, used for frequency control for the electrical grid due to the huge rotating masses of the generators and their ability to open a valve and produce more energy. However, for example, in Sweden, more than hydropower will be needed for frequency control if wind and solar are expanded to meet future energy demands [Sandberg, 2016]. Large power plants such as nuclear or coal also contribute to inertia. However, with a reduction in coal power plants, and if there is no expansion in nuclear power plants, their inertia might not be sufficient in the future to bring stability to the grid [entsoe, n.d.; Kundur, 1994].

For future energy demands to be reached using renewable energy, a proposed solution is to use batteries as backup storage and modulate inertia [Xing et al., 2021]. Using more renewable energy will require large batteries (or other forms of storage) that need to store a vast amount of energy during high production and low demand while supporting the grid when production is low and high demand. In addition, acquiring batteries can stabilize the grid frequency, meet energy demands, and increase the reliability of charging an EV [Nerve, n.d.].

The number of EVs is increasing, and their need for electricity can strain the new and the current electrical grid, especially if more vehicles become electric. The strain on the grid might be more apparent with the gradual switch to using more renewable energy. To support the grid and ensure there is always electricity for EVs, a proposed solution is to use a battery to charge the EV [Trafikanalys, n.d.].

As mentioned, large batteries are required for grid support and EV charging. These large batteries can be expensive and require a considerable investment cost. In order to cut down on the costs and resources required to create a new battery, EV batteries can be used past their end of life (EoL) in a second-life application. The EoL of a battery for an EV is usually when the current capacity of a battery has dropped to 80% of its nominal capacity [Xiong and Shen, n.d.]. The second-life applications of the batteries imply that they are used past their EoL for other applications.

To meet future demands for the electrical grid and EVs, then safe and reliable operations of batteries are necessary. To allow for safe and reliable operations of batteries, knowledge of the battery's current SoH is vital.

Goal of the thesis

This thesis aims to estimate the SoH of a Lithium Iron Phosphate (LFP) battery system.

The purpose of this battery system is to be used for grid support and as a new battery-buffered EV high-power charger. The idea is that this battery will support renewable energy to charge EVs [ApS, n.d.]. When the electricity demand is high, the battery will support the EV charger to keep it operational. The battery will be charged when renewable energy production is high, and demand is low.

There is little knowledge of the batteries used, such as the amount of charge and discharge cycles performed, their current capacity, and their current SoH. Therefore, estimating these parameters of the battery will be studied in this thesis.

The battery might deteriorate over time (calendar aging) and with use (cycle aging). How much the battery has deteriorated can be defined by the SoH. The focus of this thesis is to figure out a method to study the online SoH of the battery. Online estimation implies estimating SoH in real-time instead of extensive battery testing. Furthermore, online SoH estimation of the battery could allow for applying necessary control measures to increase the lifespan and prevent failures.

The main objective of this Master Thesis is to estimate the SoH of a battery system. The objective can be divided into the following sub-objectives.

- **State of the art analysis**
  - Review how the research front tackles SoH estimation and battery modeling of battery systems.
  - Study what methods for SoH estimation are successful.
  - Study previous research used to define the SoH.
- **Define SoH**
  - Define SoH in a way that can be tested and validated.
  - The definition for SoH needs to be relevant to the usage of the battery.
- **Derive a mathematical model of the battery**
  - Derive a model that sufficiently captures the internal dynamics of the SoC and terminal voltage of the battery regarding changes in SoH.
  - Determine a mathematical model of the battery's performance concerning SoH of the battery.
  - Create a model of an aging battery and run simulations of the aging battery.
- **Derive the estimator**

  - Derive an estimator that can estimate the necessary variables to determine SoH. Some of the variables that are accessible are the battery's internal temperature, output current, terminal voltage, and SoC.
  - the estimator requires that the estimation is fast and robust.

- **Perform experiments and validate the model and estimator**
  - Analyze the collected data and adjust the model accordingly.
  - Perform a test to see the performance of the model and the real data.
  - Validate the model with the data from the experiments.
  - Evaluate the reliability of the results from the model and experiment results.

Thesis structure

- **Chapter 2** This chapter presents the theoretical background used in the thesis. This aims to give the reader knowledge about the theory used in the thesis.
- **Chapter 3** This chapter presents and explains the methods used to acquire the battery model. The workflow of creating the model and acquiring the necessary parameters will be presented in this chapter. The choice of estimation methods used is explained in this chapter. How the estimation takes place will also be presented.
- **Chapter 4** The simulation and testing that have been done are presented in this chapter. The results are presented here.
- **Chapter 5** This chapter presents the results of the modeling, simulation, and testing of the battery system.
- **Chapter 6** In this chapter, the conclusion of the thesis is drawn from the results and the discussion. The future work of the thesis is discussed here.

2

Theoretical Background

This chapter will explain the theoretical building blocks for determining SoH. The chapter will start by introducing the main concepts that will be used regarding the battery, such as C-rate, SoC, and DoD, that are necessary to determine and define the SoH of a battery. Next, the different methods that SoH is defined and estimated in literature will be presented. Next, the problem statement will be explained, and the definitions for SoH used in this thesis will be discussed. Lastly, the chapter will discuss the relevant methods from control theory, such as EKF, WLS, and RLS.

Battery

A battery is an electrochemical device that can produce or store electricity through chemical reactions. The battery cells used in this thesis are Lithium Iron Phosphate (LFP). LFPs are not optimal for EVs due to their low power and energy density compared to other Lithium-ion batteries. The low energy density makes them heavier than other Lithium-ion batteries, which is undesirable for EVs. On the other hand, the lower energy density makes LFP batteries more suitable for storage and grid support [Couto et al., 2022]. The battery system is used for grid support and EV charging. The LFP suits well for this application.

When discharged, the battery produces DC and requires DC to be charged. Therefore, a rectifier and an inverter are needed to charge and discharge from and to the electrical grid. A rectifier converts AC into DC. An inverter converts DC into AC. Since the current in the AC changes, the battery would charge and discharge proportional to the frequency of the AC.

A current flows when a load is connected to the battery's two terminals. The potential from the two terminals is denoted by the terminal voltage (V_{term}). When there is no load on the two terminals, and they are not connected, no current flows through the battery. There is, however, still a potential, denoted by the open circuit voltage (V_{oc}) [Couto et al., 2022].

C-rate. A current rate (C-rate) of a battery is the current that it is being charged or discharged with, related to its total capacity in Ah [Couto et al., 2022].

$$C\text{-}rate = \frac{I_{discharge/charge}}{Q_{Ah}} \tag{2.1}$$

$C\text{-}rate$	The current discharge/charge rate
$I_{discharge/charge}$	The discharge/charge current in A
Q_{Ah}	The full capacity of the battery in Ah

For example, a battery with a total capacity of 100Ah being discharged at a current of 100A implies it is discharged at a $C\text{-}rate$ of 1 since it will take 1 hour for the battery to be completely discharged. If the battery is discharged with 30A, it implies that it is discharged at a $C\text{-}rate$ of 0.3 (or around C/3). It will take 3.3 hours for the battery to be completely discharged [Xiong and Shen, n.d.; Plett, 2015].

Battery capacity. The battery capacity (Q) implies the total charge that the battery contains. The battery's capacity can be defined as the total Ampere hours (Ah) or Watt hours (Wh) in the battery. When Wh is used for the battery's capacity, the term energy of the battery is commonly used. The capacity and energy will be defined as Q_{Ah} from the capacity in Ah and Q_{Wh} for the capacity in Wh. The producer gives the nominal capacity, the theoretical max the battery can hold [Xiong and Shen, n.d.; Plett, 2015].

State of Charge. The State of Charge (SoC) is defined as the current charge in the battery compared to the total capacity of the battery. For example, when a phone is charged to 80%, this implies an SoC of 80%. A common method for determining the SoC is from Coulomb counting [Xiong and Shen, n.d.; Plett, 2015], as shown in equation (2.2). The initial SoC at the beginning of discharge or charge ($SoC(t_0)$) is subtracted by the integrated current (i) during the time of charge or discharge, times the efficiency of charge or discharge (η) divided by the nominal capacity ($Q_{nom,Ah}$) in Ah as shown in the equation below.

$$SoC(t) = SoC(t_0) - \frac{1}{Q_{nom,Ah}} \int_{t_0}^{t} \eta i(\tau) d\tau \tag{2.2}$$

With equation (2.2), $SoC(0)$ and Q need to be known to determine the SoC accurately. Equation (2.2) is the same when the battery is being charged or discharged since when the battery is charged, the current is negative, and when the battery is charging and positive when the current is discharging [Plett, 2015; Xiong and Shen, n.d.].

Battery management system. The battery management system (BMS) maintains and controls the battery [Xiong and Shen, n.d.; Plett, 2015]. It is responsible for

the charging and discharging operations of the battery. The BMS ensures that the desired current and voltage are reached and that the voltage stops the charging and discharging at the battery's voltage cut. The BMS's job is to ensure the battery is safely operated. The BMS must be able to measure a battery cell's voltage, temperature, and current. The SoC must be measured, and the cells should be balanced. Balancing cells implies that the SoC and SoH are equalized, along with reaching the desired current [Plett, 2015; Xiong and Shen, n.d.; Pinter et al., 2021].

Depth of discharge. Depth of discharge (DoD) is how much the battery has been discharged compared to its full capacity [Xiong and Shen, n.d.; Plett, 2015]. Most BMS limit the DoD to 80%. This implies that with a battery of 100Ah with a DoD of 80%, the battery has been discharged with 80Ah. The DoD is usually stated at 100% SoC until 20%. The useful capacity is the capacity that can be extracted from the battery. When a battery of a capacity of 100 Ah is discharged at a DoD of 80%, which the BMS limits, the capacity is measured or estimated. The measured or estimated extracted capacity is the useful capacity. The DoD can also indicate the useful energy that can be extracted from the battery. Usable energy means how much energy can be stored in the battery or extracted within its operational range. The usable capacity is usually the energy extracted at 80% DoD [Calearo et al., 2022].

End of Life. The battery's EoL is when it can no longer meet its technical specification [Xiong and Shen, n.d.; Plett, 2015]. The end of life of a battery is usually defined when it has a capacity drop to 80% of its nominal capacity. The decrease in capacity due to aging is considered a capacity fade [Xiong and Shen, n.d.]

State of Health

The SoH describes how much the battery has aged compared to its beginning of life and how the battery age can be classified into cycle aging or calendar aging [Xiong and Shen, n.d.; Plett, 2015]. Cycle aging implies how much the battery degrades due to the charging and discharging cycles. Calendar aging implies how much the battery degrades due to the passing of time [Thingvad et al., 2021].

Reference [Birkl et al., 2017] presents the different effects on the cell when they age and why the SoH decreases. The battery can also degrade if the C-rate is too high, if the temperature is too high, or if the voltage is outside its operational range.

The capacity of the battery is expected to reduce over time and usage. The reduction in capacity is partly due to unwanted side reactions that consume the lithium. The electrode deterioration is also a cause of capacity fading [Plett, 2015].

There have been numerous ways to estimate the SoH. Unfortunately, some estimation methods are impractical for online applications due to the extensive testing needed.

SoH estimation from changes in capacity and resistance. According to [Plett, 2015], the SoH is defined as the present total capacity over the nominal capacity and

the present equivalent series resistance (ESR) over the nominal ESR. To estimate the SoH, a model needs to be created that simulates the behavior of the battery during discharge, charge, and aging. Other parameters that change when the battery's SoH changes can include the open circuit voltage (V_{oc}), but this is not widely used in current BMS to determine the SoH. Methods for estimating SoH include non-linear Kalman Filter (KF) such as Extended Kalman Filter (EKF), Sigma-point Kalman Filter (SPKF), and Joint and dual estimation [Plett, 2015]. The non-linear KF can estimate slow time-varying changes in the battery parameters that can be used to estimate the SoH. The parameters can include the present equivalent series resistance. The capacity can be determined using methods such as linear regression, Weighted ordinary least squares (WOLS), weighted total least squares (WTLS), simplified least squares (SLS), and recursive least squares (RLS) from the estimated SoC and the Coulomb counted SoC [Plett, 2015]. Once the necessary parameter have been estimated, the SoH is calculated from the change in current capacity over the nominal and the current ESR over the nominal.

[Moreno, 2021] presents three methods for estimating SoH. One is SoC-based SoH estimation. The other studies charge gradient-based SoH estimation and impedance-based SoH estimation. The first method used the two SoH relationships, as shown in the equations below.

$$SoH_Q = \frac{Q_{full}}{Q_{nom}} \tag{2.3}$$

$$SoH_R = \frac{R_0}{R_{0,nom}} \tag{2.4}$$

where Q_{full} is the current maximum available capacity, Q_{nom} is the rated capacity, R_0 is the current internal resistance, and $R_{0,nom}$ is the nominal internal resistance. Each method is tested using constant current constant voltage (CCCV). The results are compared using the incremental capacity (IC) method and differential voltage (DV) trajectory variations.

The book [Xiong, n.d.] uses a similar definition for SoH as [Xiong and Shen, n.d.] with capacity or energy measurements, internal resistance, and impedance measurement methods. They also discuss indirect measurement methods that calibrate the related SoH by studying process parameters. The process parameters can include solid electrolyte interphase (SEI) film resistance, capacity-V_{oc}-SoC response, voltage response, and charging time with constant current or voltage. They state that these can be combined to get a broader perspective of the SoH. These methods performed tests with constant current (CC), constant voltage (CV), or CCCV.

The article [Thingvad et al., 2020] defines SoH as the full current capacity (Q_{full}) compared to the nominal capacity (Q_{nom}). Therefore, the SoH is calculated through the equation below.

$$SoH = \frac{Q_{full}}{Q_{nom}} \tag{2.5}$$

The experiments are performed in a laboratory setting where the battery is discharged from 100% to 0%.

SoH approximation from cycle counting. In [Xiong and Shen, n.d.], they used several definitions for SoH. They state that SoH can be determined by the energy or capacity fade of the battery. SoH is defined in that paper as the currently available capacity or energy ratio compared to the nominal capacity or energy. They also present internal resistance measurement for the SoH estimation. With the R_0 measurement, the battery's EoL is when the current R_0 is twice that of the nominal. The present internal resistance measurement is derived from a discharge and charge pulse test. Impedance measurement could also be used for SoH estimation using electrochemical impedance spectroscopy (EIS). The impedance increases with aging and can be used for SoH estimation. For calculating the SoH using cycle number counting, the equation used is shown below:

$$SoH = \frac{N_{total} - N_{exp}}{N_{total}} \tag{2.6}$$

This method is tested using the CC and CV methods to charge the battery. They also mention destructive methods which destroy the cell to study the internal chemistry of the cell. These methods can determine the SoH of the battery with high precision but destroy the cell.

SoH estimation from decreasing initial discharge potential. The paper [Kong et al., 2018] presents two models for SoH estimation. One method includes SoH prediction based on decreasing discharge potential at the beginning of discharge (V_{0+}). The other SoH prediction method is based on the increasing constant voltage (CV) charging capacity. The purpose of studying V_{0+} is to find a mathematical model for SoH concerning temperature and charge/discharge current. One method suggests a prediction model by studying the decrease of V_{0+} as seen in equation (2.7).

$$V_{0+} = V_{0+}(n) \tag{2.7}$$

where n is the number of cycles performed on the battery and V_{0+} is the voltage at the start of the discharge. Using linear regression to relate the cycle number to the change in V_{0+}, equation (2.8) is obtained.

$$V_{0+}(n) = \beta_0 + \beta_1 n \tag{2.8}$$

β_0 is the original value and β_1 is the rate of change. The other model in [Kong et al., 2018] studies the CV charging capacity of the battery. The resistance increases from the model, so the constant current charge reaches the cutoff voltage faster with aging. Linear regression is also performed to get a function related to the cycle number of the battery.

SoH estimation from Equivalent-Hydraulic model. In [Couto et al., 2019], the SoH is estimated using a two-step approach. The first used the Equivalent-Hydraulic model (EHM) and estimated SoH using EKF and SoC. The other step attempts to link specific parameters to the degradation of the battery for online measurement of SoH. The general way of defining SoH in [Couto et al., 2019] is presented in equation (2.9).

$$SoH = \frac{\delta\theta_0}{\theta_0} \tag{2.9}$$

where $\delta\theta_0$ is the change of any variable from its initial (nominal) value θ_0. $\delta\theta_0$ is calculated using an estimated current value of a variable ($\hat{\theta}_0$) and the nominal value (θ_0) using:

$$\delta\theta_0 = \hat{\theta}_0 - \theta_0 \tag{2.10}$$

[Couto et al., 2019] compares the estimated SoH from capacity fade and power fade. The tests were carried out by testing different C-rates of the battery in a temperature-controlled climate chamber. The results were parameters related to SoH with enough precision to observe aging.

SoH estimation through V_{oc}-SoC curves. In the article [Thingvad et al., 2020], they also present a method to estimate SoH, called the V_{oc}-SoC method. The V_{oc}-SoC method is based on a curve that relates the V_{oc} to a specific SoC. This method can estimate the SoH during partial charging. To estimate the SoH, the following formula is used:

$$SoH = \frac{\Delta SoC_{CC}}{\Delta SoC_{V_{oc}}}, \tag{2.11}$$

where ΔSoC_{CC} is the difference in SoC given by coulomb counting and $\Delta SoC_{V_{oc}}$ is the difference given by the V_{oc}-SoC curve. To estimate SOH, one must estimate the SoC with the V_{oc} and perform a partial discharge. During the discharge, coulomb counting is performed, and another estimate of the SoC is made with the V_{oc}. The SoH is after that given by equation (2.11). In the characterization of SoH methods made in [Yang et al., 2021], it is noted that the V_{oc}-SoC method has some drawbacks. The V_{oc}-SoC curve requires a long period of testing to obtain, which is not very practical for use cases outside of the laboratory. In [Thingvad et al., 2021], they also confirm the long testing period required to measure the V_{oc}. To measure the V_{oc}, the terminal voltage must be measured when the relaxation time has passed, which might take hours, depending on battery chemistry. Another problem with this method is that the SoH estimation accuracy depends on the current measurement. Since the current is integrated during coulomb counting, the error will continuously grow over a long time. It is, therefore, necessary to calibrate the SoC with the V_{oc}-SoC curve when possible.

SoH estimation with integrated voltage method. In [Zhou et al., 2018], a method to estimate SoH during partial charges or discharges was used, called the integrated voltage (IV) method. While searching for an SoH estimation method that works with both CC and CV, they discovered that integrated voltage over time (equation (2.12)), during the charging phase, strongly correlates to the SoH.

$$IV = \int_{t_0}^{t_1} V_{term}\, dt \tag{2.12}$$

where V_{term} is the terminal voltage, t_0 and t_1 correspond to the time when two predefined voltages are reached. These are freely chosen, and in [Zhou et al., 2018], the two predefined voltages were chosen as $V_0 = 3.85V, V_1 = 4.2V$. The two predefined voltages are the terminal voltage at an SoC of 12% and 89%. In [Jenu et al., 2022], the two predefined voltages were chosen as $V_0 = 3.3V, V_1 = 3.4V$, and in that article, they were studying an LFP cell. The relationship between SoH and IV is assumed to be linear and given by:

$$SoH = \alpha + IV \cdot \beta \tag{2.13}$$

where α and β are parameters to be determined by the least squares method from experimental data. α is the initial SoH and β is the gradient.

SoH estimation with incremental capacity analysis. The article [Jenu et al., 2022] used incremental capacity analysis (ICA) to estimate SoH. The ICA method uses the incremental capacity (IC) curve to estimate the SoH. The following equation gives the curve:

$$IC = \frac{dQ}{dV} \tag{2.14}$$

where Q is the charged or discharged capacity, and V is the terminal voltage. In [Jenu et al., 2022], Q is given by coulomb counting:

$$Q = \int_{t_1}^{t_2} I dt \tag{2.15}$$

where t_1 and t_2 are the start and stop times of the charging or discharging period. From the ICA curve, the SoH can be determined by studying the changes in the peak area and then applying RMS to plot the results. The SoH in [Jenu et al., 2022] uses capacity fade to determine the SoH of the battery by fitting a polynomial to the IC curve. The paper [Jenu et al., 2022] also researched how the C-rate affects the SoH estimate and found that the lower the C-rate is, the better for an accurate estimation. Though, a C-rate of 2 still provided satisfactory results.

SoH estimation with ML. In the report [Wu et al., 2020], the authors use Artificial Neural Networks (ANN), which is a form of Machine Learning (ML) for predicting states in the battery to be used to determine the SoH. However, they also state the

problems of using ANN or ML, which is the vast amount of data needed to create an accurate model.

The report [Clevert et al., 2016] presents the advantages and disadvantages of using the EC model. Some disadvantages are due to the variation in R_0 being very small. R_0 being very small makes it difficult to predict using a KF accurately. Also, KF has a disadvantage in that it is difficult to apply due to the system's complexity. So instead, the report studies Deep Neural Networks (DNN) to be applied for SoH estimation.

In [Cârstoiu et al., 2021], the authors state that the usual way of defining SoH is the ratio of the current energy capacity to the nominal capacity of a fresh battery. They state that the EC model is most commonly cited, partly due to its implementation simplicity. They talk about the problems of using a Recurrent Neural Network (RNN) for SoH estimation, but the problems with the amount of time it takes for the training and that it is prone to error. They use the model for SoH from the accumulated degradation model L, where $L = 1 - SoH$.

The second method in the report [Moreno, 2021] trained an intelligent algorithm to determine SoH using equation (2.3). The third method uses equation (2.3) and (2.4) to estimate SoH using an impedance-based method. These methods use machine learning to determine the SoH of the battery.

In [El-Dalahmeh et al., 2021], the SoH is defined according to the equation below:

$$SoH = \frac{Q_{full}}{Q_{nom}} \times 100\% \tag{2.16}$$

where Q_{full} is the full current capacity and Q_{nom} is the battery's nominal capacity. The estimation technique used is based on three data-driven (DD) algorithms. They conclude that the DD algorithms are sufficient for SoH estimation, especially for online applications. They discuss the problem with the EC model, which is not accurate enough but is simple to implement. The ECh model is accurate but too complex to be implemented.

SoH definition for this thesis

There is no universal agreement for what SoH is for a battery, as discussed in the literature [Xiong and Shen, n.d.; Plett, 2015; Couto et al., 2019; Moreno, 2021]. The definition of the SoH needs to be relevant to the usage of the battery and the model, respectively. The battery will be used for grid support (GS) and EV charging stations in this thesis. If the battery is primarily used for frequency compensation, it must be able to supply enough power at a specific time. There are other frequency compensation methods for renewable energy systems, such as inverters with inertia [Hamada et al., 2022]. Suppose the battery only stores the excess generated electricity from wind turbines. In that case, it is more important to determine the total current capacity to predict how much energy can be stored in the batteries to support the grid. For EV charging stations, the capacity in Ah and Wh are essential for charging an EV.

The SoH estimation aims to see what the SoH is of a battery when the battery is received. Knowledge of the SoH is not guaranteed when it is received from an EV, for example, in a second-life scenario. Knowledge of SoH is essential to prevent failures and determine battery usage. For the battery, it is important to know what the capacity of the battery is compared to the nominal and to know the available charge that can be supported to the grid and the EV. If the available capacity becomes too low, the battery becomes useless [Kong et al., 2018].

The SoH can be accurately determined by opening up the battery and studying the internal chemistry of the battery. A problem with this method is that the battery is dismantled and can no longer be used. This method is impractical for determining the current SoH of a battery in use since it destroys the cell [Xiong and Shen, n.d.].

As mentioned in the literature, there are a couple of model-based methods for SoH estimation: The Equivalent circuit (EC) model, the electrochemical model (ECh), the data-driven model (DD), and the equivalent hydraulic model (EHM) [Plett, 2015; Wu et al., 2020; Clevert et al., 2016; Cârstoiu et al., 2021; Couto et al., 2019]. Using the (EC) model, multiple variables can be studied to estimate the SoH, and the EC is relatively easy to implement. The definition of SoH that is chosen affects what models can be chosen. The measurements that can be taken to estimate the SoH also affect the chosen model.

The EC model is a common physical battery model for SoH estimation. From the EC model, the power fades, capacity fade, change in SoC, internal resistance increase, or change in internal resistance can be estimated. These estimates can all be used to, in turn, estimate the SoH. The (EC) model has a few different layouts. The common EC models are the Thevenin model [Plett, 2015]. When there is an internal capacitance and resistance in parallel, this model is very simple but can be expanded indefinitely. The limit for expanding the EC model is the accuracy of the estimated variables and the computational time. From the EC model, the SoH can be estimated by itself or in combination with another battery model. More details about the modeling method used will be defined in chapter 3.

From the EC model, the terminal voltage of the batteries can be simulated. The model, in turn, can show how the battery behaves during charge and discharge and, in turn, see changes that could be due to the SoH. For example, as the battery degrades, the internal resistance of the battery is expected to increase, which increases the losses and lowers the total capacity. In addition, different components in the battery, such as shunt capacitance and resistance, might also vary with SoH and cause deviations in the model. Another attempt to estimate SoH is to look at the battery's total capacity (Q) and compare it to the nominal. A problem with looking at Q is that a whole cycle needs to be performed to measure the total current capacity of the cell. In normal operations, this rarely happens to the battery. It is, however, a test that can be performed. The capacity can also be estimated using the change in SoC during a short charging period and then the battery's total capacity is estimated [Thingvad et al., 2020].

The definition adopted for this thesis for SoH is the relationship between the

current capacity and its nominal capacity together with the increase in internal resistance compared to its nominal resistance. Traditionally, batteries are mainly used for discharging and not primarily for charging. Therefore, most methods for determining the total capacity are when the battery is discharged. Therefore, the battery's total capacity when charged and discharged is essential.

The SoH can be compared in Wh, Ah, SoC, and R_0. Each of the cases will be discussed in the following.

$$SoH_{Wh} = \frac{\hat{Q}_{meas,Wh}}{\hat{Q}_{nom,Wh}} = \frac{\sum_{k=1}^{N_s} i_k \hat{V}_{meas}}{\sum_{k=1}^{N_s} i_0 \hat{V}_{nom}} \tag{2.17}$$

Equation (2.17) calculates the SoH from the total power in Wh extracted from the battery and compares it to its nominal, where $\hat{Q}_{Wh}$ is the estimated capacity in Wh and calculated from the sum of the current i_k and the estimated terminal voltage $\hat{V}_{meas}$. $Q_{nom,Wh}$ is the nominal capacity in Wh and calculated from the sum of the nominal current i_0 and the nominal terminal voltage V_{nom}.

$$SoH_{Ah} = \frac{\hat{Q}_{measAh}}{Q_{nomAh}} = \frac{\sum_{k=1}^{N_s} i_k}{\sum_{k=1}^{N_s} i_k} \tag{2.18}$$

where equation (2.18) calculates the SoH from the total power in Wh extracted from the battery and compares it to its nominal, and $\hat{Q}_{meas,Ah}$ is the estimated capacity in Ah and calculated from the sum of the measured current i_k. $Q_{nom,Ah}$ is the nominal capacity in Ah and calculated from the sum of the nominal current i_0, which is also given by the technical specifications or early measurements.

$$SoH_{R_0} = \frac{R_{0,nominal}}{R_{0,current}} \tag{2.19}$$

where equation (2.19) calculates the SoH from the changes in ESR (R_0), and $R_{0,nominal}$ is the nominal ESR given by the technical specifications or early measurements, and $R_{0,current}$ is the estimated current ESR of the battery.

$$SoH_{SoC} = \frac{\Delta SoC_{calc}}{\Delta SoC_{est}} \tag{2.20}$$

where equation (2.20) calculates the SoH by dividing the change in Coulomb counted SoC (ΔSoC_{calc}) by the estimated change in SoC (ΔSoC_{est}). The definitions for SoH in equations (2.18), (2.19) and (2.20) will be used and compared.

Control Theory

Control theory methods are used to model, and estimate the parameters of the battery to determine the SoH. The extended Kalman filter (EKF) has been used to estimate the slowly varying parameters of the battery [Zucconi, n.d.; Plett, 2015]. The EKF has been used instead of the ordinary Kalman Filter (KF) because it can

handle non-linear processes. Weighted least squares (WLS) and Recursive weighted least squares (RLS) [Kutner et al., 2005] are used to determine the capacity and in turn the SoH of the battery.

To accurately control or estimate SoH, a good model of the system is necessary for accurate estimations. The more accurate the model of the actual process, the better the estimation will be. Linear systems are simpler systems to create a model of. However, in reality, few systems are linear. The system in question is a time-varying non-linear system. The nonlinearity is partly due to the complex internal dynamics of the LFP battery, not exact knowledge of the process of the system, and the change in the SoH of the battery. A change in the SoH might cause the battery to behave differently than if the SoH would not change. These changes can be hard to predict since the battery's internal chemistry is not directly observable under normal operations. The output does not follow the input proportionally, but other factors affect the systems that are not measurable or predictable. Since the output does not directly follow, the input makes it difficult to create a model since the output is not directly proportional to the input.

There are numerous ways of dealing with non-linear systems. The most simplistic method is to linearize the non-linear system. This method allows the non-linear system to be treated locally as a linear system and be modeled in such a way. Linearizing a system can be done in a couple of ways, such as linearizing around a point or a trajectory [Zucconi, n.d.].

The SoH will be estimated using control theory techniques. The estimation will be carried out by creating a model of the battery and then bringing forward the mathematical equations of the system by setting up a system of equations. The system of equations will be put in a block diagram. With the block diagram, possible disturbances will be added, and the estimation will be included.

State space representation. A system with mathematical equations can be represented in a state space form in continuous time.

$$\dot{\mathbf{x}} = A\mathbf{x} + Bu \tag{2.21}$$

Equation (2.21) shows the state transition equation, where the states are $\mathbf{x}$, the input is u, the changes in states are given by $\dot{\mathbf{x}}$ and A is the state transition matrix with dimensions $N \times N$ where N is the number of states and shows how the state $\mathbf{x}$ affects $\dot{\mathbf{x}}$. B is the input transition matrix with dimensions $N \times M$ where M is the number of input signals and B shows how the input affects the $\dot{\mathbf{x}}$.

$$y = C\mathbf{x} + Du \tag{2.22}$$

Equation (2.22) shows the measurement function, where the states are $\mathbf{x}$, the input is u, and the measurement or output is y. C is the observation matrix with dimensions $N_y \times N$ where N_y is the number of measurements or outputs, and N is the number of states and shows how the state $\mathbf{x}$ affects y. Finally, D is the feed-through matrix

with dimensions $N_y \times M$, where M is the number of input signals and D shows how the input affects y. Where $\mathbf{x}$ are all the states in the system.

For example, the output of a system could be inside room temperature. The input could be the outside temperature. The states could be people inside the room or how much heat escapes the window. The states, in this case, can be measured and can change if someone leaves the room or the window is closed. But they are all affected by the outside temperature u and affect the inside temperature y.

Kalman filter

The Kalman Filter (KF) is an optimal linear filter [Glad and Ljung, 2000]. The KF has a wide variety of applications. For example, a KF can be used for smoothing, filtering, or predicting the states of a system [Glad and Ljung, 2000]. The KF is an optimal linear state observer (or state estimator) and assumes Gaussian noise [Glad and Ljung, 2000]. For example, due to technical limitations such as the measuring equipment can not handle high heat such as rocket heat, or when the states are not actual components but made up components to capture the dynamics of a process, state observers (or estimated states) can be used in the such cases.

The KF uses the current states of the model and the current measurements to study the difference between the states and the measuments. The KF starts with an initial estimate of the states and the estimation error covariance. A new state is predicted and attempts to minimize the error in the estimated state. This process is then updated as new measurements are received and the actual states of the system change [Automatic Control LTH, n.d.].

The sampling time is a property of the KF, and the more frequently the time is sampled, the better the approximations of the continuous system are. In discrete time the KF has a prediction step and a state update step [Glad and Ljung, 2000].

Prediction step:

$$\hat{x}_{k|k-1} = F_{k-1}\hat{x}_{k-1|k-1} + B_{k-1}u_{k-1} \tag{2.23}$$

$$P_{k|k-1} = F_{k-1}P_{k-1|k-1}F_{k-1}^T + Q_{k-1} \tag{2.24}$$

Update step:

$$K_k = P_{k|k-1}H_k^T(H_kP_{k|k-1}H_k^T + R_k)^{-1} \tag{2.25}$$

$$\hat{x}_{k|k} = \hat{x}_{k|k-1} + K_k(y_k - H_k\hat{x}_{k|k-1}) \tag{2.26}$$

$$P_{k|k} = (I - K_kH_k)P_{k|k-1}(I - K_kH_k)^T + K_kR_kK_k^T \tag{2.27}$$

$\hat{x}_{k\|k-1}$	The predicted state k based on $k-1$ measurements
$\hat{x}_{k-1\|k-1}$	The state estimate at $k-1$
$\hat{x}_{k\|k}$	Estimated state at k
u_{k-1}	The input at $k-1$
y_k	The measurement at k
F_{k-1}	The state state transition matrix at $k-1$
B_{k-1}	The input transition matrix at $k-1$
H_k	The observation matrix at k
$P_{k\|k-1}$	Covariance matrix at k based on $k-1$
$P_{k-1\|k-1}$	Covariance matrix at $k-1$
$P_{k\|k}$	The updated covariance matrix at k
K_k	The Kalman gain at k
Q_{k-1}	Process noise matrix at $k-1$
R_k	The measurement uncertainty or noise at k
I	Identity matrix

Measurement noise variance. The measurement noise variance is the variance of the noise that affects the measured output of our system. The measurement noise can be caused by uncertain measurements or such as disturbances. The origin of these disturbances could be white noise from the measurement equipment. R represents the measurement noise variance. The measurement noise is assumed to be uncorrelated Gaussian noise.

Process noise variance. The process noise variance is the noise that affects the input in the system and, in turn, the process. In this case, the input is current, so the noise could be errors in the measurement of the current or disturbances when the battery switches some cells on and off. The process noise variance of the system affects the system of equations and the states of the system. Therefore, the process noise variance is represented using Q. The process noise is assumed to be uncorrelated Gaussian noise.

Extended Kalman Filter

An extended Kalman Filter (EKF) is a KF modified to handle non-linear processes. It is necessary to calculate the conditional expectation of the state. The conditional expectations are calculated by calculating $\hat{x}$, linearizing around the current $\hat{x}$, and calculating the Kalman gain at the current instant. When the state and measurement dynamics are linearized, the result is an EKF.

The EKF is structured similarly to the KF but with the state estimate being linearized around the current estimate.

$$f(x) \approx f(\hat{x}_0) + f'(\hat{x}_0)(x - \hat{x}_0) \tag{2.28}$$

Equation (2.28) approximates a linear function to the non-linear data to estimate the state $\hat{x}$. The linearization is done with an initial state estimate $\hat{x}_0$ and a function $f(\hat{x})$

that aims to be the same as $f(x)$. Then, the slope of the function is given by $f'(\hat{x}_0)$ that is multiplied by the estimated state $\hat{x}_0$ and the actual state x. This linearization is done at every new estimate of the state $\hat{x}$. Once the dynamics are linearized, the prediction equations are the same as for the KF with equations (2.23) and (2.24). The update equations are the same as for the KF with equations (2.25), (2.26), and (2.27) [Zucconi, n.d.].

Weighted least squares

Weighted least squares (WLS) [Plett, 2015] are used when the relationship between x and y is unknown, and x and y are two data sets. WLS attempts to find a relationship with some function $y = f(x,r)$ between these sets of data points by minimizing the residual (r) and, in turn, minimizes the cost function (2.29). The residual is the difference between y and $f(x,r)$ [Strutz, 2016]. With WLS, the residual is weighted using the variance of the data points. The variance weighs the importance of the residual and affects the changes in $f(x,r)$ more or less. The weight w is often defined as the inverse variance ($\frac{1}{\sigma^2}$) of the data points in y.

$$\chi^2 = \sum_{i=1}^{N} \frac{(y_i - f(x_i,r))^2}{\sigma_{y_i}^2} \tag{2.29}$$

where χ^2 is the cost function. The derivative of function (2.29) with respect to the function $f(x,r)$ is shown in equation (2.30)

$$\frac{\delta\chi^2}{\delta f(x,r)} = -2\sum_{i=1}^{N} \frac{(y_i - f(x_i,r))}{\sigma_{y_i}^2} \tag{2.30}$$

Equation (2.29) and (2.30) are combined to determine the function $f(x,r)$ [Plett, 2015].

Recursive weighted least squares

Recursive weighted least squares (RLS) [Plett, 2015] are similar to WLS. The main difference is that the weight is updated at each iteration when new data arrives. The iteration allows for more or less importance to the error. The recursion is performed by updating the weight each time new data is received. The purpose is to localize the weight at each time instance and adjust so that the variance can be larger at different times. In the WLS, the weight is usually the inverse variance ($\frac{1}{\sigma^2}$). In the RLS, the inverse variance is updated at every time instance and results in ($\frac{1}{\sigma_i^2}$) at every time instance [Plett, 2015].

3

Method

This chapter will first describe the assumptions made and the limitation of the thesis. Next, the tools used to gather the data and run the experiments are described. Then, the derivation of the different models used and how they work will be discussed. Lastly, the estimation techniques using WLS and RLS and how they will be validated will be explained.

Assumptions

The ambient temperature of the battery is not controllable. However, the ambient temperature in the lab does not significantly change. The temperature difference in the lab is between 18 and 30°C during the time of the tests. The operating range of the cells is 0-70°C during charge and -20 to 70 °C during discharge. However, the cells behave quite differently if they are at 25°C or 45°C. Since the change in ambient temperature is low, the ambient temperature change is assumed not to affect the cells. The battery's assumed parameters, such as resistors and capacitors, are temperature-dependent, affecting the current and the voltage. As the battery is being charged and discharged, the temperature change is assumed to be small enough not to affect the resistance and capacitance. The values for the components have been assumed to be at a constant 25°C.

The amount of charging and discharging cycles performed on the battery is assumed to affect the SoH of the battery to a more considerable extent than the calendar aging over a short period. The experimentation lasts for five months. The battery should degrade less than 0.63% [Wang et al., 2022] in five months. The battery in this study has more than 2000 life cycles. The lifetime implies that it can be charged and discharged more than 2000 times with a DoD of 80% at 0.3 C until the battery has reached its end of life. If the battery is charged and discharged with a higher C rate, it might degrade at a higher rate. The battery will be charged and discharged at around 0.375 C and an 80% DoD. This project has assumed that the battery will only degrade due to cycle aging. The project expects the number of cycles to degrade the battery more significantly than the degradation due to the passing of time. Other ways a battery can degrade could be from mechanical damage or a significant

increase or decrease in temperature that can affect the internal chemistry of the battery. This project has assumed that this will not and has not happened to the battery. Damages to the cell can increase the cell's aging and therefore change the SoH at a higher rate. The battery can also degrade if the C-rate is too high or the voltage exceeds the operational range. The battery will not be operated at a high C-rate, and the BMS should ensure the voltage is within its operational range. The assumption is that the battery will not degrade due to too high a current or voltage outside the operational range, only from normal operations.

The open circuit voltage (V_{oc}) is essential to create an accurate model since the terminal voltage output depends on the V_{oc}. However, for LFP batteries, the V_{oc} does not change significantly with changes in SoH [Plett, 2015]. Therefore, data of the batteries V_{oc} to SoC exists and is assumed to not change with changes in SoH.

Delimitations

The project is limited to DTU's power lab. The experiments are at DTU's power lab. The experiments take a long time to perform, and avoiding scheduling conflicts with other projects is necessary. Avoiding scheduling conflicts requires synchronization with different projects to perform the test without disturbance.

Controlling the temperature of the cells is not possible. How the temperature changes internally in the cell is not directly measurable. There are temperature sensors on the top of each cell, but they are assumed to differ from the internal temperature of the battery.

Running tests on other types of batteries is not possible. Therefore, the model and estimation are limited to the LFP battery system in the lab. The measurements and tests aim to be applicable in real-world applications to determine the SoH. However, the limitation in measurements might cause difficulties in accurately estimating SoH. In addition, the real-world operations of the battery might also differ from the lab and cause the battery to degrade faster or slower than expected, for example, due to larger temperature changes or higher or lower C-rates.

The battery that the experiments were carried out on has its own BMS. The BMS can not be changed or modified. Balancing the batteries in the BMS can cause nonlinearity and make the estimations difficult. Testing on individual cells is impossible with the current setup, but acquiring data from individual cells is possible. Not being able to test on individual cells limits the accuracy of not having a controlled environment.

The battery cells in the battery system will differ slightly due to imperfections in the production stage. The assumption is made that all cells are initially the same and have the same values for the parameters of the cell.

Due to the current energy crisis in Europe, DTU, including DTU power labDK, might be shut down for a process called a brownout. A brownout is an intentional blackout that is implemented in emergencies. If Denmark's energy production reaches a critical low, then DTU might be subjected to a brownout to supply more

important facilities with energy. A brownout will limit the amount of testing that can be done on the battery as the electricity supply is cut out. The brownout is not intended to be long-lasting, but if it occurs in the middle of a charge/discharge cycle test, some data will be lost, and the test will be ruined.

Lab setup

The experiments are in a lab in a big room where multiple other experiments are being conducted. This project is limited to a lab cell connecting the battery, electrical grid, and power amplifier. There is also a connection between the battery, the Nerve smart system, and a Raspberry Pi to communicate with the battery. The data from the battery is accessed remotely and stored on a computer, where it is processed. The lab setup is illustrated in Figure 3.1. The battery is not directly connected to the local grid but is passed through the inverter and rectifier.

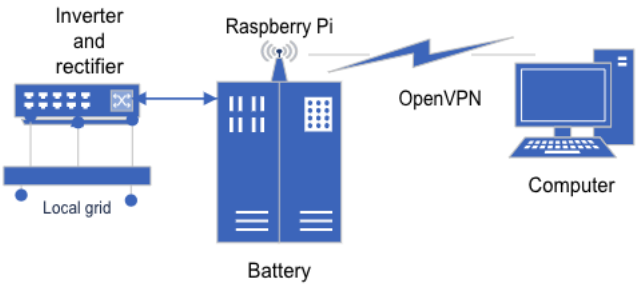

Figure 3.1 Diagram of the lab setup

PowerLabDK. The experimentation is at PowerLabDK in the laboratory at DTU [PowerLabDK, n.d.]. It is a world-class facility for performing experiments on electric power and energy. In addition, the facility hosts experiments on renewable energy research or research that contribute to cost-efficient, reliable, and sustainable power systems based on renewable sources. In PowerLabDK, one can find the state of the art laboratories for many different areas, such as the electric vehicle lab, the high power lab, the high voltage lab, and more [PowerLabDK, n.d.]. However, the experiments in this thesis are in the electric lab and lab cell 9.

PuTTY and automation. PuTTY is a terminal simulator that supports SSH and Telnet for Windows and Linux-based platforms [Tatham, n.d.]. The client connects to the Raspberry Pi via SSH, which controls the BMS. In addition, scripts are in the programming language bash through PuTTY, which can control the BMS.

UaExpert. UaExpert is an OPC UA client used to log the experiment data measurements [Foundation, n.d.]. OPC is a standard used within industrial automation for secure and reliable data exchange [Foundation, n.d.]. UaExpert subscribes to

different values generated by the measurement equipment, and every time a value is updated, a generation of a new data point occurs in UaExpert. After generating a new data point, adding the data point to a CCV file with a maximum of 10.000 lines occurs. A new CCV file is generated when it reaches the maximum number of lines.

SCADA. SCADA software controls circuit breakers in the lab cells [OleumTech, n.d.]. With this software, one can control all the circuit breakers for certain laboratories within PowerLabDK. In addition, it can open and close breakers remotely and get an overview of the electrical grid at PowerLabDK.

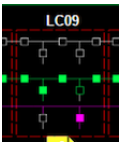

Figure 3.2 The lab cell used for testing the batteries in SCADA

Figure 3.2 shows the lab cell in SCADA. The controller for the battery is the purple circuit breaker in lab cell 9 (LC9), and the green circuit breaker in LC9 is where the charging and discharging current goes through.

MATLAB® and Simulink®. MATLAB® is a programming language developed by Mathworks [MathWorks, n.d.]. MATLAB® is used to represent the state-space model. In addition, MATLAB® is used to process the raw data received from UaExpert, so it is possible to perform simulations. Finally, MATLAB® is also used to perform necessary calculations and estimate the capacity.

Simulink® is a tool that simulates processes such as the battery system. First, using block diagrams, Simulink® is used to simulate the real process of the battery. Next, Simulink® will be used with MATLAB® to simulate the battery and estimate the values.

NERVE smart systems. The BMS of the battery is from NERVE smart systems [Nerve, n.d.]. The calculated SoC by the NERVE smart systems uses Coulomb counting. As the NERVE smart system attempts to estimate the SoC, an error grows over time. To reset the error, the SoC needs to be calibrated occasionally. The calibration occurs at the edges of SoC, so close to 0% and 100% SoC. But when the calibration is necessary is not known to the author [Nerve, n.d.; Pinter et al., 2021].

Battery cell. The battery cell is a Sinopoly SP-LFP100AHA battery cell [*Sinopoly battery systems* n.d.]. The battery is charged and discharged at around 0.375 C, equivalent to 37.5 A. The capacity used to calculate the C-rate of the battery uses 100Ah. However, charging or discharging the capacity at 0.375 C increases the capacity to around 107Ah.

Rectifier and inverter. The rectifier and inverter are essential to charge and discharge the battery system to and from the grid. The rectifier and the inverter are a Coverdan 3-phase active front-end module [*Coverdan* n.d.] The rectifier and inverter are needed because the battery system can only charge and discharge with DC, and the grid has AC. The rectifier and inverter limit the battery's charge or discharge C-rate. The limit in C-rate is because the rectifier and inverter have a fuse of 50A. If the current is larger than 50A, a fuse will break, or it might damage the rectifier and inverter [*Coverdan* n.d.].

Test deployment

The testing consists of charging and discharging the battery. A script charges the battery to the maximum allowed SoC and discharges to the lowest allowed SoC. One full charge and discharge is considered one cycle. The cycles are looped continuously with a break between a charge and discharge session of 30 min, as seen in Figure 3.3. The reason for the break is to allow the battery to cool and for the diffusion voltages to settle to their steady-state values. The longer the break is, the longer the battery has to settle, but then a cycle takes longer. The waiting time compromises the quality and quantity of the measurements. To reach the desired power at the start of a charge and discharge, the script has a ramp function, which slowly increases the current at the start of the charge and discharge. The reason for the ramp function is to avoid overshooting the current that might cause a fuse in the inverter and rectifier to break.

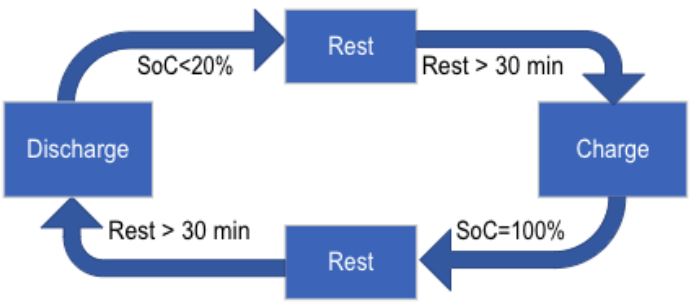

Figure 3.3 Flow chart of the test algorithm

The testing is on the entire battery system. For one cycle, all 295 cells are charged and discharged. However, the balancing algorithm in the BMS does not charge and discharge all cells simultaneously. Instead, the charging and discharging are stopped and started to keep the desired voltage of around 800V for the whole battery system. Even though the batteries are all connected in series, the Nerve smart system allows a cell to be bypassed and stop charging or discharging for individual

cells. Connecting the cells in series implies that the current in all cells switched on is the same.

Modeling

Modeling the battery is a vital part of this thesis. The more accurate the model of the battery is, the more accurate the estimations will be. There are a few models to consider when creating a model of the battery. These include the electrochemical (ECh) model, the equivalent circuit (EC) model, or the data-driven (DD) model [Plett, 2015; Wu et al., 2020; Clevert et al., 2016; Cârstoiu et al., 2021; Couto et al., 2019]. The ECh model is, according to the literature, the most accurate model for SoH estimation. The ECh model is, however, very complex, takes a lot of computational power, and requires difficult measurements. The complexity makes the model slow and not very practical for online applications. Simplified ECh models use half of a cell that requires less computational power but with a loss of accuracy [Couto et al., 2022]. The lab setup is impractical for an ECh model since the experiments are on a whole battery pack, not just one or half a cell. The DD model can give accurate results and quick results. Its application is good for a black box where the states are unknown or the nominal SoH of the battery. The major problem with the DD model is that it requires a lot of data to create an accurate prediction. The vast amount of data required will be a problem due to the limited time for testing [Glad and Ljung, 2000].

The model chosen was the EC model due to its simplicity, the measurements of the battery system, and the limit in the amount of data required to create the model. Creating a model was done by deriving mathematical equations of the process, creating a model, and testing the model. Then, the model was updated, and necessary changes were made depending on the results. Finally, battery cell models are modified to handle charging and discharging. The reason for this is that the battery behaves slightly differently from charging or discharging. The difference between charging and discharging is due to the components of the EC model being different for charging and discharging.

EC model. There is a couple of different way of designing the EC model. To model a battery as an equivalent circuit, a certain amount of building blocks to capture the dynamics are needed [Plett, 2015]. The idea of an EC model is to represent the battery's behaviors with known or similar electrical components. The simplest EC model of the battery is an RC model. When $n = 0$, the model consists of just a voltage source V_{oc}.

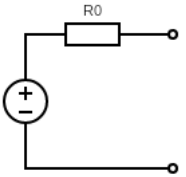

Figure 3.4 An 0-RC EC model

When $n = 1$, the model consists of one branch of a resistor R and a capacitor C in parallel called the RC branch. The RC components exist to catch the behavior of the diffusion voltage of the battery. For example, the model in Figure 3.5 is a 1-RC model of the battery.

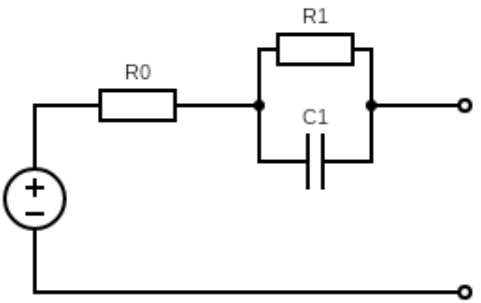

Figure 3.5 An 1-RC EC model

The model in Figure 3.5 uses an ideal voltage source with internal resistance and a resistor and capacitance in parallel. The purpose of the resistance and capacitance of the battery is to catch the behavior of the battery. This model can be expanded to better catch the behavior of the battery by adding more parallel resistance and capacitance. This model is considered an n-RC model when $n > 1$. This expansion makes it more complex but increases the accuracy of the model.

According to [Xiong and Shen, n.d.], the error decreases with an increase in n. The computational time, however, becomes huge when n is higher than 4. When n is smaller than 4, the model gives a high accuracy with a short computational time. Adding more states can also lead to problems related to overfitting and might

cause problems in predictions and estimations [B.S. Everitt, 2010]. The difficulty in deriving the parameters for the n-RC circuit increases for higher orders of n. The 2-RC model will be used to have high accuracy but not too computationally demanding. A 2-RC circuit is illustrated in Figure 3.6. The 2-RC model consists of an ideal voltage source denoted V_{oc}, and R_0, two branches of a resistor and capacitor in parallel denoted R_1, C_1 and R_1 and C_2, respectively.

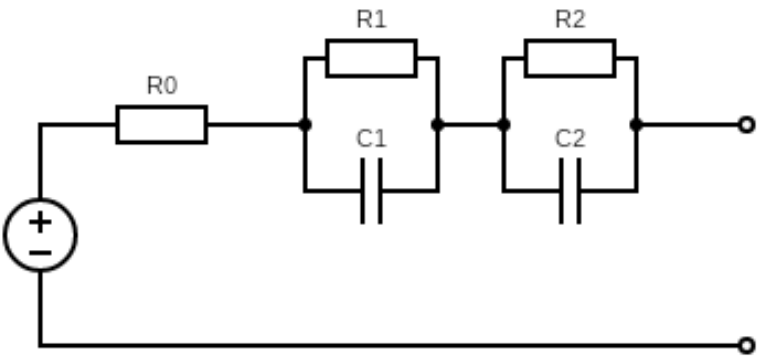

Figure 3.6 An 2-RC EC model. R0 is the internal resistance. R1 and C1 exist to capture the diffusion voltage, and R2, and C2 exist to extend the capture of the diffusion voltage.

Resistance estimation. The equivalent series resistance (R_0) can be estimated by studying changes in terminal voltage over the change in current for the same time interval. Since the current changes very little, to estimate the R_0, the change in current and voltage needs to be captured when the change in current and voltage are relatively significant, for example, when the cell is switched on and off. Switching on and off an individual cell is not possible [Plett, 2015]. The cell is, however, switched on and off as the BMS attempts to balance the voltage to 800V. Studying the response of a cell being switched on and off could be enough to estimate R_0.

$$R_0 = \frac{\Delta V}{\Delta I} \tag{3.1}$$

From equation (3.1), ΔV is the change in voltage, and ΔI is the change in current. This method should be avoided when ΔI is small (in CC charge or discharge) since it will be a division by a number close to zero, and the resistance will be infinite. Since ΔI needs to be large, equation (3.1) only works when the cell is switched on or off. There is data on how R_0 changes with SoC but not with changes in SoH.

Resistance-capacitor couples. A similar test to deriving R_0 could be performed to determine variables such as R_1, R_2, C_1, and C_2. Determining the variables is more complicated since the resting time required is around 30 min [Plett, 2015]. There are lookup tables from [Pinter et al., n.d.; Schmidt et al., n.d.] based on SoC for the values of V_{oc},R_0, R_1, R_2, C_1, and C_2 for a cell that has been used to create the model with an assumed constant temperature of 20°C [Pinter et al., n.d.; Schmidt et al., n.d.].

The resistance in the resistance-capacitor couples represents the charge transfer resistance R_n [Ω], and the capacitors C_n [F] represent the internal dynamics of the battery that can be observed as a time delay. The time delay in the system $\tau(s)$ equals RC [Plett, 2015].

The resistor and the capacitor in parallel values can be determined using the pulse test and studying the slow change in voltage as the terminal voltage reaches its steady state. Determining the resistor and the capacitor values is tedious and takes a long time. Acquiring the values at a high precision limits the degree of the n-RC circuit. Most reports use no more than a 2-RC circuit, and some use less. The values for the components of R and C in the 2-RC will not be determined and have been acquired from previous research of a similar cell [Pinter et al., n.d.; Schmidt et al., n.d.]. The reason for not deriving them is the limitation in the testing equipment for individual cells. Performing an accurate pulse test for the whole system would be time-consuming, tedious, and error-prone.

The nominal capacity. The nominal capacity of the cells is 100Ah. However, this is dependent on the C-rate for charging and discharging.

A higher C-rate of the battery lowers the capacity. Since the battery is discharged at around 30A or 37.5A, the operational battery range is between 2.8V and 3.8V. The capacity at the battery's lower cut-off voltage of the cell was estimated to be around 107Ah. 107Ah is what is used as Q_0 for the battery at a discharge rate of around $\frac{C}{3}$. The nominal useful capacity is the nominal capacity that can be extracted from the battery. The useful capacity is approximately 80% of the full capacity. As the nominal capacity is estimated to 107Ah, the useful nominal capacity is 85.6Ah. The capacity of 107Ah is an assumption based on the technical specifications of the battery. To gain better knowledge of the battery cell, then testing on the cell is required at the start of life.

First-principles modelling. The measurements of the battery are the terminal voltage, the current, and the outer cell temperature. The battery's resistors or capacitors are components in the system that can not be measured directly and have to be estimated. The components that comprise the EC model, such as the R_0 and the resistance and capacitance in parallel, are taken from previous experiments on a similar cell with the same battery chemistry [Pinter et al., n.d.; Schmidt et al., n.d.].

There are two different models: the degrading model and the tracking model. The purpose of the degrading model is to simulate how the battery degraded depending on the number of cycles. The development of a tracking model was a more

iterative procedure where the first version was the 2-RC model with an EKF, the second the model with SoC as a state, and the final version was the model of 2-RC and SoC as the only state in the EKF.

Assuming a 2-RC circuit, the terminal voltage can be determined by the sum of all the voltages in the circuit, following Kirchhoff's voltage law, as seen in equation (3.2). A 2-RC circuit is illustrated in Figure 3.6.

$$V_{term} = V_{oc} - V_0 - V_1 - V_2 \tag{3.2}$$

V_{term}	Terminal voltage of a cell
V_{oc}	Open circuit voltage of a cell
V_0	Voltage over the R_0
V_1	Voltage over the first RC branch
V_2	Voltage over the second RC branch

Ohm's law can be used to determine the voltage over R_0 as shown in equation (3.3).

$$V_0 = R_0 i \tag{3.3}$$

The relationship between capacitance, voltage, and current is shown in equation (3.4).

$$i_C = C\frac{dV}{dt} \tag{3.4}$$

where i_C is current over the capacitor, C is the capacitance of the capacitor, and $\frac{dV}{dt}$ is the change in voltage multiplied by the capacity. For example, in a parallel RC circuit, the current over the parallel coupling is illustrated in equation (3.5).

$$i = i_R + i_C \implies i_R = i - i_C \tag{3.5}$$

where i_R is current over the resistor and the voltage over the resistance is shown in equation (3.6).

$$V_{RC} = i_R R \tag{3.6}$$

Inserting equation (3.6) in iR and equation (3.4) in i_C results in equation (3.7).

$$V_{RC} = i_R R = R(i - i_C) \implies V_{RC} = R\left(i - C\frac{dV_{RC}}{dt}\right) \tag{3.7}$$

By rearranging equation (3.7), the final result is equation (3.8).

$$\frac{dV_{RC}}{dt} = \frac{1}{C}i - \frac{1}{RC}V_{RC} \tag{3.8}$$

The system states are according to equation (3.9) where $x_1 = V_1$ and $x_2 = V_2$. The input of the system is $u = i$.

$$V_{RC} = x \implies \frac{dV_{RC}}{dt} = \dot{x} \tag{3.9}$$

$$\dot{x} = -\frac{1}{R_1 C_1} x + \frac{1}{C_1} u \tag{3.10}$$

$$\begin{bmatrix} \dot{x}_1 \\ \dot{x}_2 \end{bmatrix} = \begin{bmatrix} -\frac{1}{R_1 C_1} & 0 \\ 0 & -\frac{1}{R_2 C_2} \end{bmatrix} \begin{bmatrix} x_1 \\ x_2 \end{bmatrix} + \begin{bmatrix} \frac{1}{C_1} \\ \frac{1}{C_2} \end{bmatrix} u \tag{3.11}$$

where R_1 and C_1 are the resistance and capacitance in the first branch. R_2 and C_2 are the resistance and capacitance in the second branch.

The states are the components that represent the internal dynamics change of the system. In the 2-RC circuit, each component is dependent on the SoC. These include R_0, R_1, R_2, C_1, C_2 and V_{oc}.

The tracking models

This section presents the method for deriving the models used to track the behavior of the battery.

2-RC model with an EKF. The 2-RC model was the first model created to see how well it could follow the existing system. The input to the system using the EC 2-RC model is the current ($u = i$) into the system. The system states are the diffusion voltages $x_1 = V_1$ and $x_2 = V_2$. The state update equation is shown in equation (3.12).

$$\dot{\mathbf{x}} = A\mathbf{x} + Bu \tag{3.12}$$

$$A = \begin{bmatrix} -\frac{1}{R_1 C_1} & 0 \\ 0 & -\frac{1}{R_2 C_2} \end{bmatrix} \tag{3.13}$$

$$B = \begin{bmatrix} \frac{1}{C_1} \\ \frac{1}{C_2} \end{bmatrix} \tag{3.14}$$

where $\mathbf{x}$ is a vector of the states x_1 and x_2 and equation (3.13) presents the state transfer matrix A. The input transition matrix B is shown in equation (3.14).

The system's output is the open circuit voltage subtracted by the terminal voltage. The desired output from the circuit is the terminal voltage, but since the open circuit voltage does not have a derivative dependence, it is not part of the state space equations. The V_{oc} is determined through a lookup table where V_{oc} depends on SoC. The system's output is shown in equation (3.20).

$$y = V_{terminal} - V_{oc} \tag{3.15}$$

$$y = C\mathbf{x} + Du \tag{3.16}$$

The observation matrix C is shown in equation (3.17).

$$C = \begin{bmatrix} -1 & -1 \end{bmatrix} \tag{3.17}$$

The feed-through matrix D is just R_0 since there is only one input into the system.

$$D = -R_0 \tag{3.18}$$

The EKF then uses the measured terminal voltage of the cell V_{term} and subtracts V_{oc} to acquire the same y as in equation (3.20).

$$SoC_{k+1} = SoC_k - \frac{100}{Q_{nom,Ah}} i_k \Delta t \tag{3.19}$$

SoC is calculated using Coulomb counting. First, the current i_k is measured at instant k for charging or discharging. Δt is the system's sampling rate, and for the measurements, $\Delta t = 1s$. The nominal capacity $Q_{nom,Ah}$ is multiplied with 3600 to get from Ah to seconds. $i_k \Delta t$ is divided by $Q_{nom,Ah}$ to get the change in SoC. The change in SoC is subtracted from the previous SoC. The initial condition for SoC is 100% for discharging and 20% for charging to follow the actual process.

All the variables in the A, B, C, and D matrices change with SoC. The variable dependency on SoC implies that the matrices change with SoC. First, all the matrices are computed and then inserted into the variable state-space system. The output of the system is y, but the terminal voltage $V_{terminal}$ is what is required, so V_{oc} is added to y to acquire $V_{terminal}$ from the model. The reason for combining $V_{terminal}$ and V_{oc} is because of the model's simplicity since V_{oc} is a time-varying constant.

$$V_{terminal} = y + V_{oc} \tag{3.20}$$

The Extended Kalman filter uses the measured $y_{measured} = V_{term,measured} - V_{oc}$. $y_{measured}$ is the actual measured output of the battery, not the output from the model. Therefore, $y_{measured}$ and input are inserted into the EKF. The EKF outputs the estimated states of the system to filter the signal and give a better V_{term} than the model. The EKF uses the same varying A, B, C, and D matrices as the model to consider changes in SoC. V_{term} from the model, the EKF estimated states and the measurements are then compared to see how well they perform.

Model with SoC as a state. By studying the 2-RC model, it was observed from the simulations and results that some improvements could be made. The attempt to create a model that follows the measured V_{term} better was to add another state in the system of equations. In this model, an extra state is added to the system of equations. The third state is the SoC and is denoted as x_3. The state transition equation is shown in equation (3.21).

$$x_3(k+1) = SoC(k+1) = SoC(k) - \frac{1}{Q_{nom}} i(k) \Delta t \tag{3.21}$$

$SoC(k)$ is the SoC at the instance k, and $SoC(k+1)$ is the next value of the SoC, Q_{nom} is the nominal capacity, and Δt is the sampling time of the current, which is 1 second. A function V_{oc} depending on the SoC is created to use SoC as a state. To make V_{oc} depending on the SoC, was accomplished by linearization around a point in the V_{oc} vs. SoC curve. The linearization resulted in equation (3.22).

$$V_{oc} = V_{oc}(base) + \alpha(SoC - SoC(base)) \tag{3.22}$$

The V_{oc} vs. SoC curve is split into ten different SoC sections, from 10% to 20%, 20% to 30%, until 100% SoC. The $V_{oc}(base)$ and $SoC(base)$ are the base of each section. α is the gradient of the straight line between two base points, for example, between $V_{oc}(base)$ at 10% SoC and $V_{oc}(base)$ at 20% SoC. The gradient of the V_{oc} vs. SoC section is α that changes for every time interval with its corresponding $V_{oc}(base)$ and $SoC(base)$. The original $V_{oc}(SoC)$ and the linearized curve are shown in Figure 3.7. Equation (3.22) is then inserted into equation (3.23), as seen in equation (3.24).

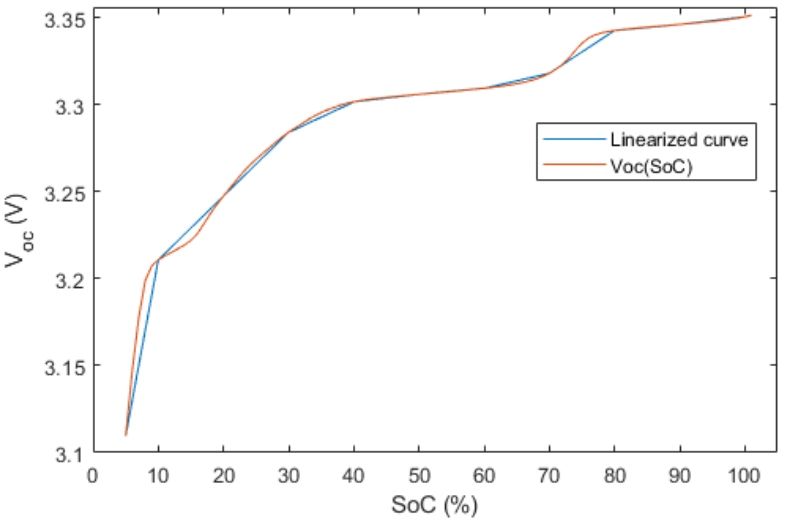

Figure 3.7 The linearized curve in blue and the original $V_{oc}(SoC)$ curve in orange

$$V_{term} = V_{oc} - V_1 - V_2 - R_0 i \tag{3.23}$$

$$V_{term} = V_{oc}(base) + \alpha(SoC - SoC(base)) - V_1 - V_2 - R_0 i \tag{3.24}$$

The variable $\alpha, V_{oc}(base)$ and $SoC(base)$ is dependent on the current SoC, $V_{oc}(base)$ is subtracted, and $SoC(base)$ is added on both sides to represent it in state space form easily. The system's output then results in equation (3.25).

$$y = V_{term} - V_{oc}(base) + \alpha SoC(base) = \alpha SoC - V_1 - V_2 - R_0 i \tag{3.25}$$

The output of the system is y, but the terminal voltage $V_{terminal}$ is what is desired, so $V_{oc}(base)$ is added and $\alpha SoC(base)$ is subtracted from y to acquire $V_{terminal}$ as seen in equation (3.26). The reason for this is the simplicity of the model. $V_{oc}(base)$ and $\alpha SoC(base)$ are values that are independent of the states dependent on the current SoC.

$$V_{term} = y + V_{oc}(base) - \alpha SoC(base) \tag{3.26}$$

The state update equation is shown in equation (3.27).

$$\dot{\mathbf{x}} = A\mathbf{x} + Bu \tag{3.27}$$

The new state transfer matrix A is shown in equation (3.28). The system states are the diffusion voltages V_1, V_2, and SoC.

$$A = \begin{bmatrix} -\frac{1}{R_1 C_1} & 0 & 0 \\ 0 & -\frac{1}{R_2 C_2} & 0 \\ 0 & 0 & 1 \end{bmatrix} \tag{3.28}$$

$$B = \begin{bmatrix} -\frac{1}{C_1} \\ -\frac{1}{C_2} \\ -\frac{\Delta t}{Q} \end{bmatrix} \tag{3.29}$$

$$y = C\mathbf{x} + Du \tag{3.30}$$

The new C matrix for equation (3.30) is shown in equation (3.31). The D matrix is the same with the new state as is shown in equation (3.32).

$$C = [-1 \ -1 \ \ \alpha] \tag{3.31}$$

$$D = -R_0 \tag{3.32}$$

Including the new state $x_3 = SoC$ is the only method to calculate the SoC for this model. The state x_3 determines the variables that make up the matrices in the system of equations. The new state x_3 calculates the SoC in the same way as in the previous model, as is shown in equation (3.21).

The EKF used for state estimation in this model also contains the new state and the new system of equations. The reason for adding the new state is to see if the SoC could estimate the states and SoC with higher accuracy if the SoC is used in the EKF compared to Coulomb counting. The estimated states in the EKF can also be used to compare to the state in the model.

Model of 2-RC and SoC as the only state in the EKF. There was some improvement in adding a third state to the system from the simulations and results. However, the estimated state in the EKF behaved unexpectedly and outside the norm. In order to improve the results, the third state x_3 was removed, and the only states are V_1 and V_2. The EKF was applied to a model with one state, which is SoC. The error with the third state might be because the states that represent V_1 and V_2 are in Volts, while the state that represents SoC are in %. The use of different units in the EKF might make it difficult for the EKF to distinguish between the states, how much they affect the output in the system, and how much they correlate.

The system of equations is the same as in the first model but with a different EKF. The measured output y that is inserted in the EKF is shown in equation (3.33).

$$y = V_{term} - V_{oc}(base) + \alpha SoC(base) - V_1 - V_2 \tag{3.33}$$

For the model, the system of equations is identical to equation (3.13), (3.14), (3.17) and (3.18).

The EKF only has the SoC as a state and the same input, which is current ($u = i$). The output (y) that enters the EKF differs from the model. Equation (3.25) must be rearranged to only depend on SoC and the current I. Moving all other variables to the left side of equation (3.25) results in equation (3.34).

$$V_{term} - V_{oc}(base) + \alpha SoC(base) + V_1 + V_2 = \alpha SoC - R_0 i \tag{3.34}$$

$$V_{term} = y + V_{oc}(base) - \alpha SoC(base) - V_1 - V_2 \tag{3.35}$$

V_{term} is then acquired from equation (3.33) by adding $V_{oc}(base)$ and subtracting $\alpha SoC(base)$, V_1 and V_2 from y as seen in equation (3.35). In this case, the A matrix for the EKF is $A = 1$, the B matrix results in $B = -\frac{\Delta t}{Q}$, the C matrix results in $C = \alpha$, and the D matrix results in $D = -R_0$. The variables in the model were determined using the SoC state from the EKF that is applied on the model.

Degrading Model

A model of a degrading battery was created. This model aims to get an idea of how the battery behaves when it degrades. The degrading model can also be used to validate the results of the other models. The validation only works if the degrading model is accurate. How the cells degrade is not precisely known. The data sheet of the battery cells states that the battery's lifetime is more than 2000 cycles at 80% DoD discharge as mentioned in Chapter 2. The end of life is, as mentioned in Chapter 2, when the battery has dropped to 80% total capacity compared to the nominal capacity. Since the assumption is made that the battery degrades linearly, a straight line can be fitted to the curve, and how the battery degrades can be modeled. The model switches between charging and discharging when its fully charged to 100% or discharged to 20%, which implies a DoD of 80%.

The drop in capacity is not expected to happen instantly but gradually as the battery is charged and discharged with a gradient of $\frac{0.2 \cdot 107}{2000} = 0.0107$. After 2000 cycles, the battery capacity will have dropped from 107Ah to 85.6Ah.

The cycles are calculated by starting at the first cycle with a cycle length of 171.2Ah in the first cycle. The cycle length decreases as the capacity in the battery decreases. When the Coulomb counting has reached the capacity length, the cycle counter is increased by one. The capacity decreases with every cycle, so the Ah required to charge the battery decreases as well with every cycle. The model is described by equation (3.36).

$$Q = Q_{nom} - \frac{0.2 \cdot Q_{nom}}{2000} n \tag{3.36}$$

where Q is the capacity after n cycles in Ah, Q_{nom} is the nominal capacity, and n is the number of cycles performed. The reason for relating the current total capacity to the number of cycles is that the capacity changes after every cycle, and the time it takes for the battery to be charged decreases with time in the degrading model as the battery degrades.

The SoH is calculated in the degrading model by calculating the current capacity over the nominal. The nominal capacity used here is 107Ah. Changes to R_0 to changes in SoH were implemented in the degrading model to get a more accurate output from the model. R_0 is expected to increase with degradation as seen in equation (3.37).

$$R_0(SoC, SoH) = R_0(SoC) \left(\frac{1}{SoH/100} \right) \tag{3.37}$$

where R_0 charges with SoC and SoH is in %.

The system of equation for the degrading model is the same as the model with SoC as a state, so equation (3.24), (3.28), (3.29), (3.31) and (3.32). The state $x_3 = SoC$ determines the matrices in the system of equations. The changes in the matrices also take into consideration the SoH. The degrading model does not use an EKF for state estimations. The B and D matrices change when SoH changes, but A and C do not change when the SoH changes. The matrices B and D change with SoH because the capacity Q in the B matrix changes with SoH, and R_0 changes with SoH.

Estimation

Estimation occurs in the EKF, where the states are estimated, as discussed in the models. From the models, the terminal voltage is filtered and acquired. The results from the models have been used to estimate the capacity and, in turn, the SoH.

Estimating capacity and energy from Coulomb counting and power counting. The simplest method for estimating the useful current capacity in both Ah and in Wh is Coulomb counting and Watt counting is shown in equations (3.38) and (3.39), respectivley.

$$\hat{Q}_{u,Ah} = \Delta t \sum_{k=1}^{N_s} i_k \tag{3.38}$$

Equation (3.38) shows how the useful capacity in Ah is calculated by summing up the current i_k until N_s. The N_s is one discharge or charge period. Δt is the sampling rate which is 1. The absolute value of the current i_k is considered for the equation to work for both discharging and charging.

$$\hat{Q}_{u,Wh} = \Delta t \sum_{k=1}^{N_s} i_k V_{meas,k} \tag{3.39}$$

Equation (3.39) shows how the useful capacity in Wh is calculated by summing up the current i_k multiplied by the terminal voltage V_{meas} until N_s. Δt is the sampling rate which is 1. The N_s is one discharge or charge period. The absolute value of the current i_k is considered for the equation to work for both discharging and charging.

The purpose of using both equations (3.38) and (3.39) is to compare and see if the change in capacity is different when considering Ah and Wh. The capacity in Wh, is also helpful to see how much total power the battery can contain. This method determines the cell's useful capacity during one charge and discharge. The useful capacity can be used to calculate the total capacity if the changes in SoC during a charge and discharge are known. The changes in SoC must be known because the BMS might switch off a cell before it is fully charged or discharged to balance the voltage.

Estimating capacity from RLS and WLS. The SoC uses the capacity to calculate the current SoC of the cell, as in equation (3.19). The models that do not use SoC as a single state in the EKF made it challenging to estimate the SoC. The model that uses a single state in the EKF could be used to estimate the SoC. The EKF attempts to minimize the error between the model and the measurements. Equation (3.19) that is used for the model could have a different capacity, or the current could be slightly different due to losses or measurement errors. These differences could cause the model to deviate from the system's output. The EKF studies the system's measured output and attempts to correct the SoC. From the difference between the Coulomb counting and the estimated SoC, the deviations could be due to the capacity deviating from the actual. Coulomb counting in sections is presented in equation (3.40).

$$y_i = -\Delta t \sum_{k_i=1}^{k_{i_{end}}} i_k \tag{3.40}$$

where k_i is a section of SoC, for example, when SoC is between 10% and 20%, k_1 is the time in seconds between SoC 10% and 20%. $k_i = 1$ is the first value in the interval i and $k_{i_{end}}$ is the last value in the interval i. Δt is the sampling rate which is 1. y_i is Coulumb counted during the interval k_i.

$$x_i = SoC(k_i(1)) - SoC(k_i(end)) \tag{3.41}$$

$$y_i = Qx_i + \Delta y_i \tag{3.42}$$

The interval of k_i in equation (3.41) is the same as in equation (3.40). x_i is the change in SoC in the interval k_i. The inverse capacity Q relates x to y as seen in equation (3.42). The values of y_i and x_i are then used in WLS and RLS to fit a function between them. Equations (3.40) and (3.41) are derived from equation (3.19).

$$y_i = \beta_0 + \beta_1 x_i \tag{3.43}$$

The gradient of the curve is β_1, which is the inverse capacity. The y-intercept is β_0. WLS attempts to minimize the error between the estimated function and the measured y_i.

$$c_{1,i} = \sum_{i=1}^{n} \frac{x_i^2}{\sigma_{y_i}^2} = c_{1,i-1} + \frac{x_i^2}{\sigma_{y_i}^2} \tag{3.44}$$

$$c_{2,i} = \sum_{i=1}^{n} \frac{x_i y_i}{\sigma_{y_i}^2} = c_{2,i-1} + \frac{x_i y_i}{\sigma_{y_i}^2} \tag{3.45}$$

With RLS, the values of c_1 and c_2 are updated after every iteration as seen in equation (3.44) and (3.45). Updating c_1 and c_2 is what is considered here as the recursive version of WLS. The capacity is estimated using c_2 and c_1 after the RLS has gone through all i.

$$\hat{Q} = \frac{c_2}{c_1} \tag{3.46}$$

The estimated capacity is denoted $\hat{Q}$. The equation (3.46) shows how the capacity can be estimated from the values c_1 and c_2.

The capacity can also be estimated using the gradient to the function from the WLS. For WLS, the function fitlm() in MATLAB® is used to fit a weighted linear regression model to the two data sets x_i and y_i, where the weights are a vector w_i which is the inverse variance of y_i ($\frac{1}{\sigma_{y_i}^2}$). The variance of y_i ($\sigma_{y_i}^2$) is calculated using equation (3.47) for every instant of i.

$$\sigma_{y_i}^2 = \sqrt{\frac{(y_i - \bar{Y}_i)^2}{i}} \tag{3.47}$$

where $\bar{Y}_i$ is the mean of y_i from start until the current value of i. The reason for using both methods is to see which method gives the most likely results. The WLS assumes that there is only measurement noise on y_i but not on x_i, while RLS might handle measurement noise on both y_i and x_i better [Plett, 2015]. An advantage of the

WLS and the RLS method is that it gives the actual total capacity of the battery, not just the useful capacity. The function fitlm() returns the function as seen in equation (3.43).

Validating the model. The estimation will then be validated to determine the model's goodness of fit. To determine the goodness of fit, R^2 is a common method [Kutner et al., 2005]. How to determine R^2 is shown in equation (3.48).

$$R^2 = 1 - \frac{RSS}{TSS} \tag{3.48}$$

The total sum of squares (TSS) is presented in equation (3.49).

$$TSS = \sum_{1}^{n} (y_n - \bar{Y})^2 \tag{3.49}$$

where $\bar{Y}$ is the mean of y_n. The residual sum of squares (RSS) is presented in equation (3.50).

$$RSS = \sum_{1}^{n} (y_n - (\beta_1 x_n + \beta_0))^2 \tag{3.50}$$

where n is the amount of data points.

The standard deviation of residual (σ_R) is given in equation (3.51).

$$\sigma_R = \sqrt{\frac{RSS}{DoF}} \tag{3.51}$$

where the degrees of freedom (DoF) is $DoF = n - 2$, and n is the number of data points, since the comparison is made between two dimensions, then two is subtracted by the number of data points to acquire the DoF [Kutner et al., 2005].

4

Results

This chapter will present the acquired results. First, the estimation of R_0 is presented. Then the results of the different models are presented. The chapter finishes by presenting the capacity estimations. First, the results of the capacity estimation from Coulumb counting are presented, then the capacity estimation from RLS and WLS and the validation of the methods.

The engagement signal from the BMS is necessary for the model to work. The engage signal shows when the cells are on and off in the battery pack. However, the engagement signal from the recorded data was entirely off. The engagement error could be an error in the data processing. The engagement error was solved by taking the SoC signal and creating an engagement signal. Creating the engagement signal from SoC was done by looking at when the SoC was changing, then the cell was engaged, and when SoC was not changing, the cell was bypassed.

Estimating the equivalent series resistance. How the equivalent series resistance (R_0) changes with degradation is essential for an accurate model and observing degradation. Data is available on R_0, but only an assumption on how it changes with degradation [Pinter et al., n.d.]. An accurate estimation will better explain how R_0 behaves with degradation.

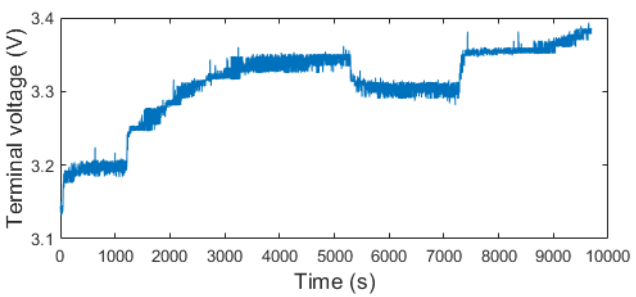

Figure 4.1 The results of measured V_{term} of a charging cell.

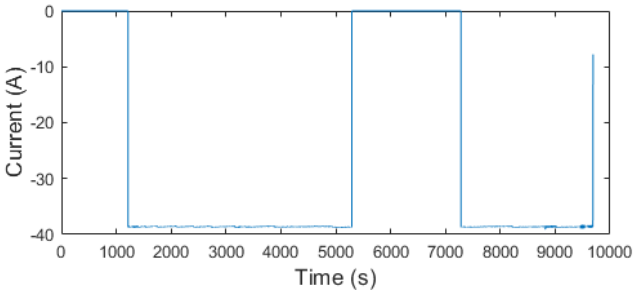

Figure 4.2 The results of measured experienced current of a charging cell.

Figure 4.1 shows the terminal voltage, and Figure 4.2 shows the experienced current of the same cell. Figure 4.1 and 4.2 show that when the current is switched on or off, the voltage changes significantly. The significant change in current and voltage is used to estimate the R_0. The diffusion voltages can also be observed, for example, at around 5200s, where the voltage decreases quickly and slowly converges when the cell is switched off. Then when it is turned on again, it rises to the same voltage as before it was switched off.

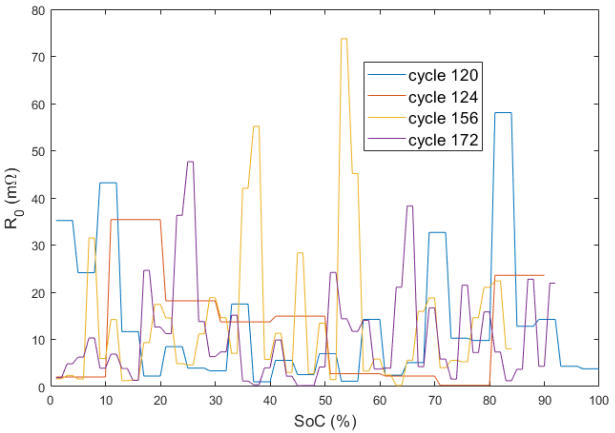

Figure 4.3 Estimating R_0 of a cell for different cycle numbers during one charge.

The data was first estimated using equation (4.1) and then filtered using equation (4.2), and the results are shown in Table 4.1.

$$\hat{R}_{0,k} = \frac{\Delta v_k}{\Delta i_k} \tag{4.1}$$

where $\hat{R}_{0,k}$ is the current R_0 estimate at the short interval k. Δv_k is the change in voltage during the short interval k. Δi_k is the change in current during the short interval k. The estimation of R_0 is taken each time the current changes significantly when the cell is turned off or on during a charge. Therefore, the estimates of R_0 were only taken during the charging of the battery.

$$\hat{R}_{0,k}^{filt} = \alpha \hat{R}_{0,k-1}^{filt} + (1-\alpha)\hat{R}_{0,k} \tag{4.2}$$

After the estimation of $\hat{R}_0$, then $\hat{R}_0$ was filtered using equation (4.2) [Plett, 2015], where α is $0 << \alpha < 1$. The α chosen was 0.95 to give more weight to the filtered data than the unfiltered. The reason for α=0.95 is that there are not a lot of data points, so a smaller α will allow for faster conversion since there are not a lot of data points for R_0 during a charge or discharge. Equation (4.2) uses the previous filtered $\hat{R}_0$ and then adds on a weight of the new. The larger α is, the more weight is put on the previous filtered value of R_0.

Table 4.1 Results of the filtered estimated R_0.

Cycles	$\hat{R}_{0,k}^{filt}$ (mΩ)
120	12.87
124	8.88
156	13.31
172	11.85

The nominal value for R_0 is 0.7 mΩ. The values for R_0 that was used for the modeling are presented in Figure 4.4.

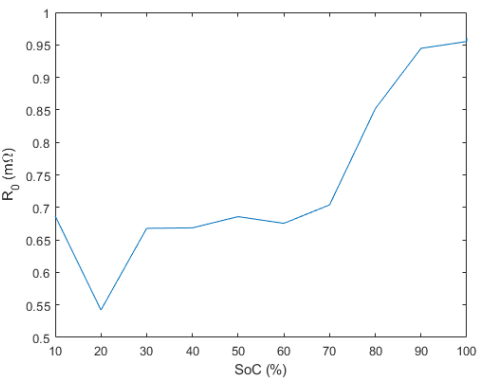

Figure 4.4 R_0 that was used instead of the estimated R_0 [Pinter et al., n.d.].

The tracking models

This section presents the results from the models that are meant to track the behavior of the battery. The results presented are of the same cell.

2-RC model with an EKF. When the cells are switched on or off during discharge, or the charge cannot be controlled during testing, the power can be set, which sets the current.

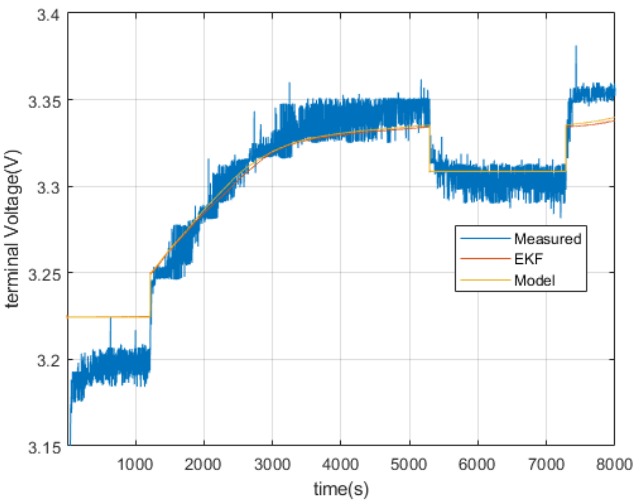

Figure 4.5 In the charging cell, blue is measured, red is EKF, and yellow is models V_{term} for the 2-RC model with an EKF.

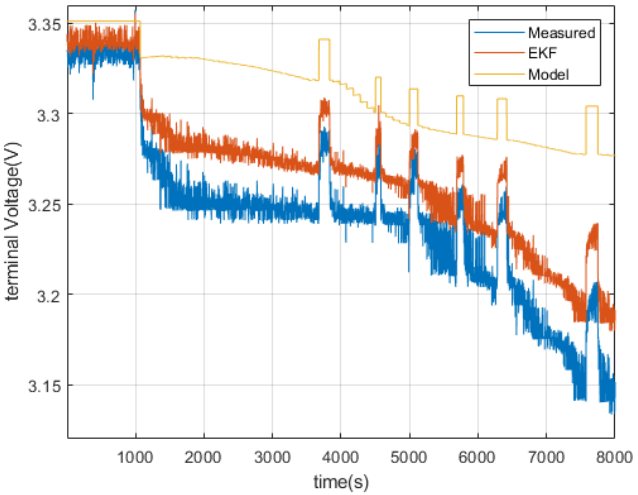

Figure 4.6 In the discharging cell, blue is measured, red is EKF, and yellow is models V_{term} for the 2-RC model with an EKF.

The results of the 2-RC model with an EKF are shown in Figure 4.5 for when the battery is charging and in Figure 4.6 for when the cell is discharging. The model does not follow the process when the cell is discharging. The only method for knowing the SoC in this model is by Coulomb counting the measured current. The model and the EKF V_{term} makes a visible compromise between measurement and model for discharging. The error between the model and the measurement for discharging seems larger than for charging. The model seems not well to fit the tested cell.

Model with SoC as a state. The model with SoC as a state has three states in the model and the EKF, as discussed in Chapter 3.

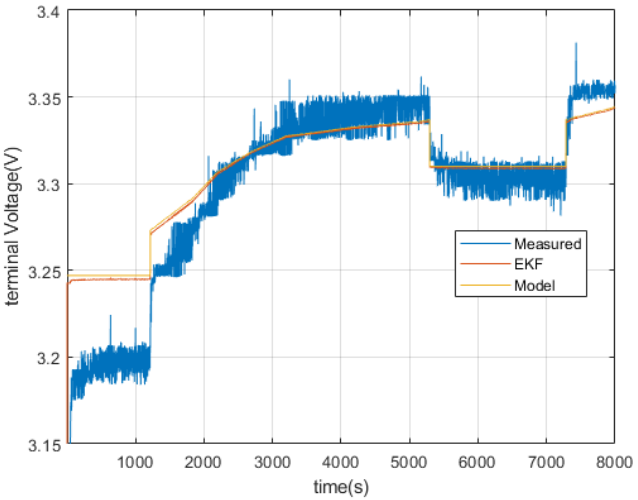

Figure 4.7 In the charging cell, blue is measured, red is EKF, and yellow is models V_{term} for the model with SoC as a state.

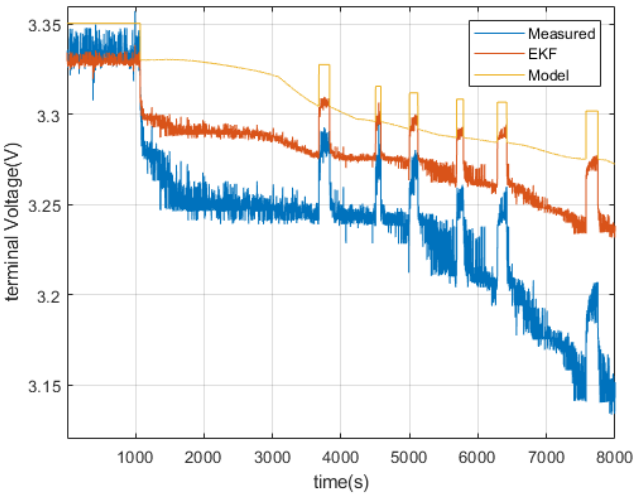

Figure 4.8 In the discharging cell, blue is measured, red is EKF, and yellow is the model's V_{term} for the model with SoC as a state.

The results of the 2-RC model with an EKF are shown in Figure 4.7 for when the battery is charging and in Figure 4.8 for when the cell is discharging. The model and the EKF with SoC as a state follow the measurements worse than the 2-RC model with an EKF for charging, as seen in Figure 4.7. On the other hand, the discharging seems to be very similar, but with the EKF V_{term} being closer than the measurements and with a lower noise magnitude as seen in Figure 4.8 than the 2-RC model with an EKF. The model and the EKF follow the terminal voltage V_{term} worse than the model without SoC as a state.

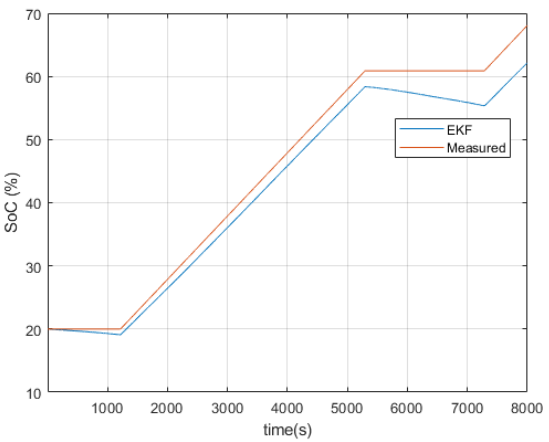

Figure 4.9 The results of SoC for the charging cell, blue is EKF, red is model (Coulumb counted) for the model with SoC as a state.

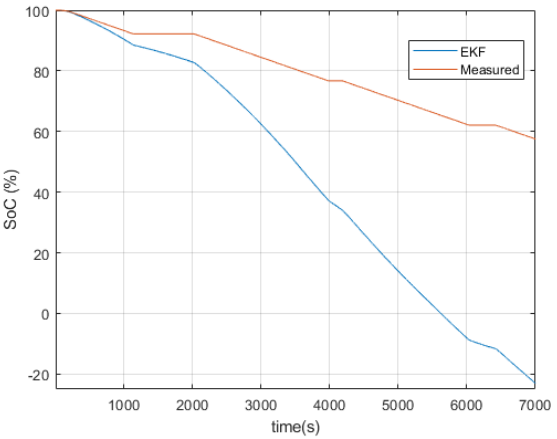

Figure 4.10 The results of SoC for the discharging cell, blue is EKF, red is model (Coulumb counted) for the model with SoC as a state.

The results of the 2-RC model with an EKF are shown in Figure 4.9 for when the battery is charging, and Figure 4.10 for when the cell is discharging. The SoC is shown here from the model's state and the estimated state from the EKF. The estimated SoC from the EKF seems to follow the SoC curve from the model well for charging, as seen in Figure 4.9. On the other hand, discharging the results for the estimated SoC seems unreasonable, as seen in Figure 4.10, since a negative SoC is not possible.

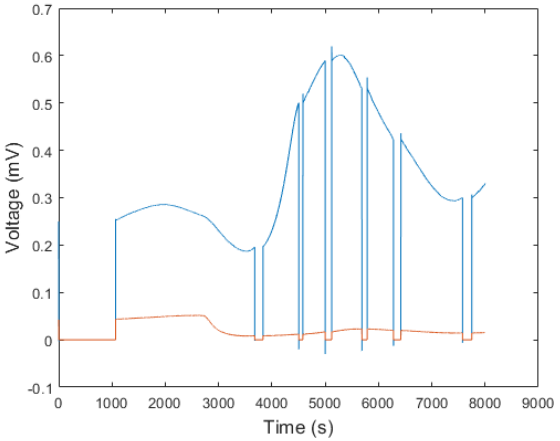

Figure 4.11 The states x_1 (in blue) and x_2 (in orange) from the model for a cell being discharged.

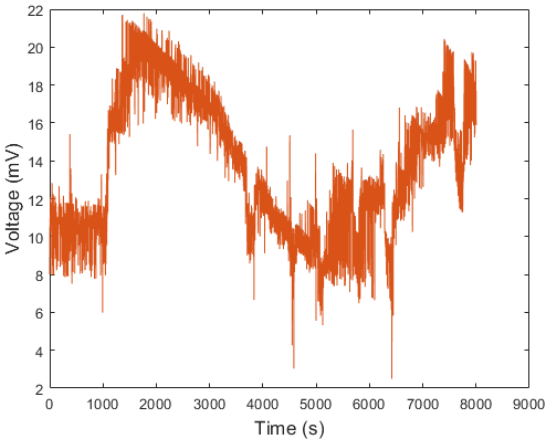

Figure 4.12 The states x_1 (in blue) and x_2 (in orange) from the EKF for a cell being discharged. The two estimated states are the same, so only x_2 (in orange) is visible.

Figure 4.11 shows how the diffusion voltages V_1 and V_2, which are the states x_1 and x_2, behave in the model. Figure 4.12 shows how the estimated diffusion voltages $\hat{V}_1$ and $\hat{V}_2$, which are the states $\hat{x}_1$ and $\hat{x}_2$, behave in the EKF. The two estimated states are the same, so only x_2 (in orange) is visible. The estimated states differ from the model states by a factor of three.

Model of 2-RC and SoC as the only state in the EKF. The model with SoC as a state has two states in the model and one in the EKF, as discussed in Chapter 3.

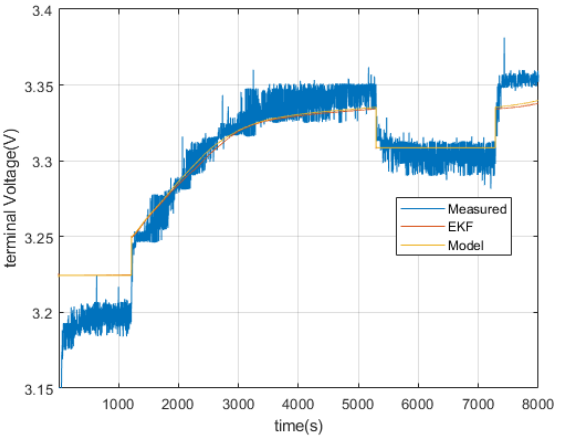

Figure 4.13 Results for the charging cell, blue is measured, red is EKF, and yellow is models V_{term} from the model of 2-RC and SoC as the only state in the EKF.

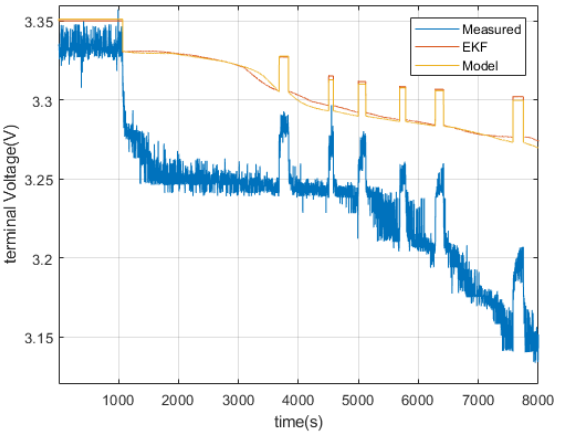

Figure 4.14 Results for the discharging cell, blue is measured, red is EKF, and yellow is models V_{term} from the model of 2-RC and SoC as the only state in the EKF.

The charging cell in Figure 4.13 is very similar to the plot for the model with

SoC as a state in Figure 4.7. The discharging cycle for this model shown in Figure 4.14, looks very different from the discharging plot for the model with SoC as a state in Figure 4.8.

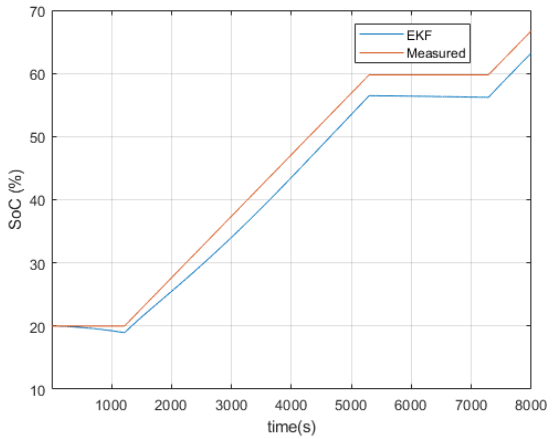

Figure 4.15 The results of SoC for the charging cell, blue is EKF, red is Coulomb counted from the model of 2-RC and SoC as the only state in the EKF.

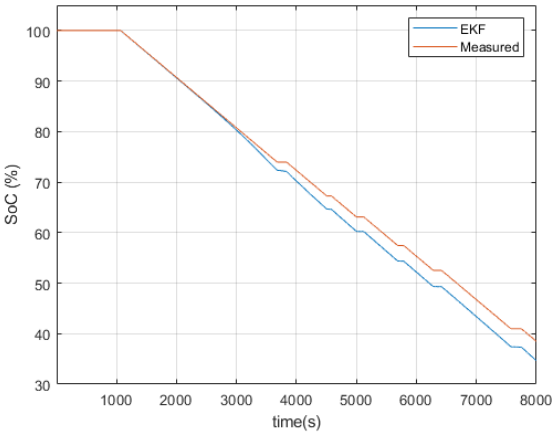

Figure 4.16 The results of SoC for the discharging cell, blue is EKF, red is Coulomb counted from the model of 2-RC and SoC as the only state in the EKF.

The SoC can be computed in two different ways in this model. First, the SoC

can be acquired from Coulomb counting. The other is the estimated SoC from the EKF. The estimated SoC from the EKF seems to follow the SoC curve better with only one state in the EKF than with three states in the model and three states in the EKF. The SoC computed from Coulomb counting and estimation for a charging cell can be seen in Figure 4.15 and for a discharging cell in Figure 4.16. The difference between the EKF and Coulomb counted SoC seems to be larger than for the discharging cell.

Degrading model

The degrading model attempted to simulate how a battery would degrade as it was being cycled. The results of simulations of the change in terminal voltage of the battery as it is being cycled and charged are presented in Figure 4.17 and for discharging in Figure 4.18.

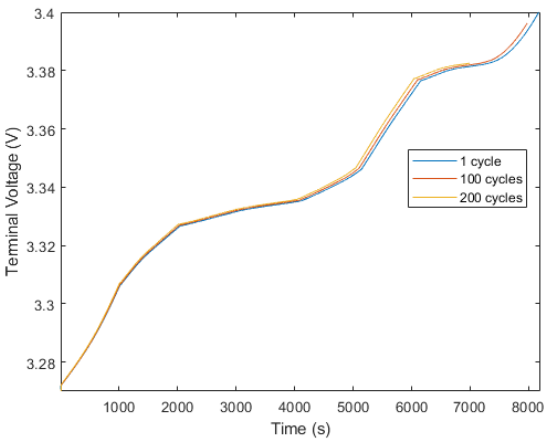

Figure 4.17 The results of V_{term} for the charging cell, blue is 1 cycle, red is 100 cycles and yellow is 200 cycles from the degrading model.

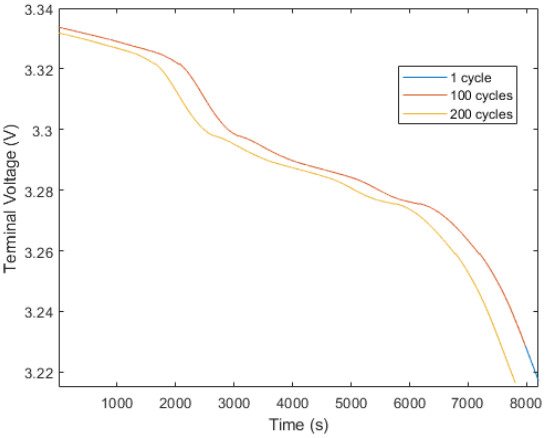

Figure 4.18 The results of V_{term} for the discharging cell, blue is 1 cycle, red is 100 cycles and yellow is 200 cycles from the degrading model.

The simulated degrading model has a DoD of 80%. The terminal voltage V_{term} behaves similarly, even with degradation. However, it stops earlier for a cell with a higher number of cycles than the one with a lower number of cycles. The terminal voltage is shorter for a degraded cell for the charging and discharging cells. The result of the simulated capacity for a different amount of cycles run is presented in Table 4.2.

Table 4.2 The results of the capacity from the degrading model

Cycles	$Q_{u,ch}$(Ah)	$Q_{u,ch}$(Wh)	$Q_{u,dis}$(Ah)	$Q_{u,dis}$(Wh)
1	85.59	286.08	85.58	281.72
100	82.91	277.03	83.11	273.73
200	80.48	267.68	81.30	267.45

The result of the simulated SoH for a different amount of cycles run is presented in Table 4.3.

Table 4.3 The results of the SoH from the degrading model

Cycles	$SoH_{Ah,ch}(\%)$	$SoH_{Wh,ch}(\%)$	$SoH_{Ah,di}(\%)$	$SoH_{Wh,dis}(\%)$
1	99.99	99.99	99.99	99.99
100	96.86	96.83	97.09	97.15
200	94.02	93.56	94.98	94.92

The nominal used capacity in Ah ($Q_{u,nom,Ah}$) to calculate the SoH is 80% of the nominal capacity $Q_{nom,Ah}$ = 107 Ah, so $Q_{useful,nom,Ah}$= 85.6 Ah.

The nominal used capacity in Wh used for charging is ($Q_{u,nom,Ah}$) to calculate the SoH is 80% of the nominal capacity $Q_{nom,Wh}$ = 357.63 Wh so $Q_{useful,nom,Wh}$= 286.1 Wh.

The nominal used capacity in Wh used for discharging is ($Q_{u,nom,Wh}$) to calculate the SoH is 80% of the nominal capacity $Q_{nom,Wh}$ = 352.19 Wh so $Q_{useful,nom,Wh}$= 281.75 Wh.

Parameter identification

To estimate the states in the different models, an EKF has been used. The EKF allowed for state estimation for a non-linear system to correct the model error. Besides using an EKF to estimate the states, the capacity was estimated to determine SoH.

Estimating capacity and energy from coulomb counting and power counting. The results presented in Figures 4.19, 4.20 4.21, 4.22, 4.23 and 4.24 are from the measurements of all the cells in the battery system.

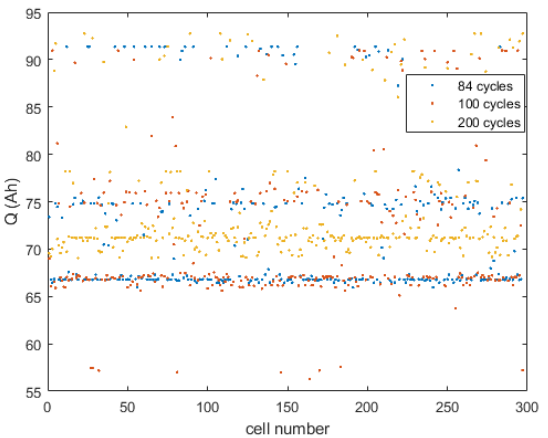

Figure 4.19 The results of useful Q in Ah all cells for three different cycles for the charging battery.

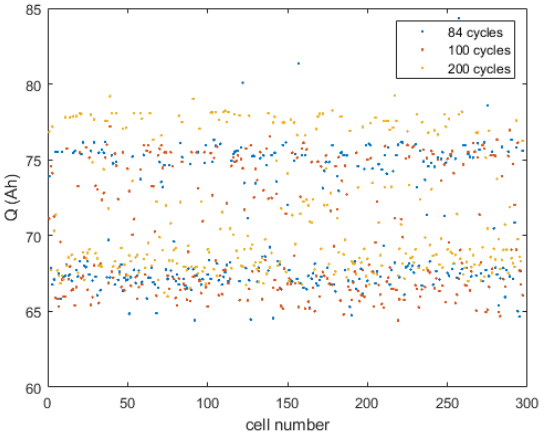

Figure 4.20 The results of useful Q in Ah all cells for three different cycles for the discharging battery.

Figures 4.19 and 4.20 show the capacity of all 297 cells after being tested for 84, 100 and 200 cycles. The cells look to have formed two or three groups with a capacity of around 67Ah, 75Ah, and 90Ah for a charging battery. When the battery is discharging, then the capacity seems more spread out.

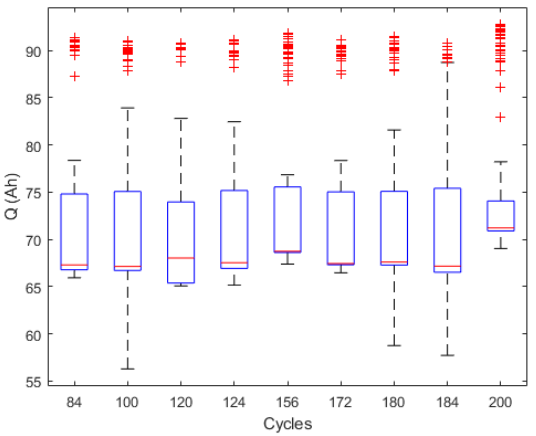

Figure 4.21 The useful capacity of a charging cell in Ah for all cells in the battery.

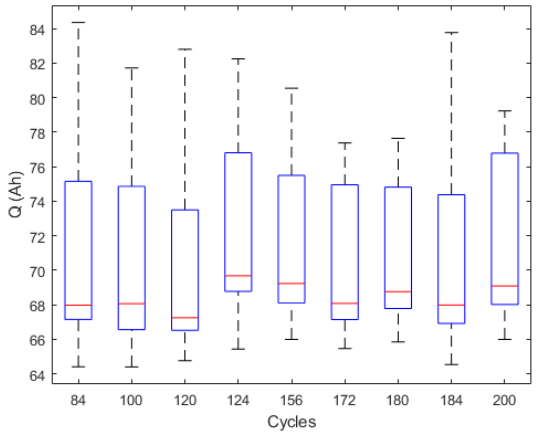

Figure 4.22 The useful capacity of a discharging cell in Ah for all cells in the battery.

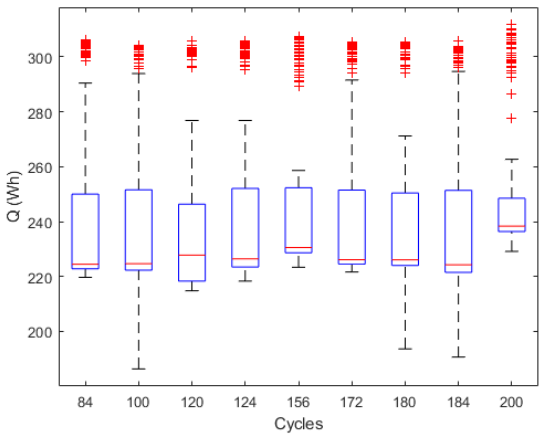

Figure 4.23 The useful capacity of a charging cell in Wh for all cells in the battery.

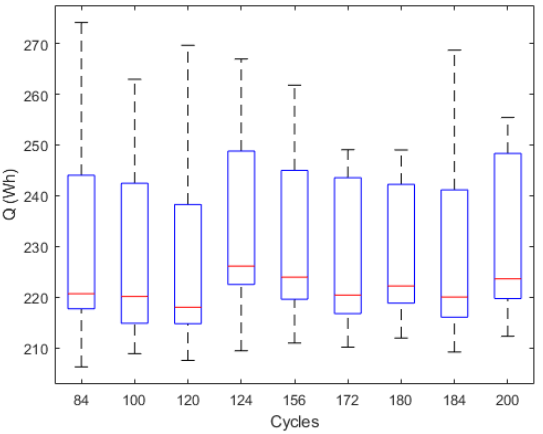

Figure 4.24 The useful capacity of a discharging cell in Wh for all cells in the battery.

In Figures 4.21, 4.22, 4.23 and 4.24, all the useful capacities from all the cells are shown in Ah and Wh for charging and discharging cells. The black dotted line above the box shows the upper adjacent. The black dotted line below the box shows the lower adjacent. The bottom of the box shows the 25th percentile. The top of the box shows the 75th percentile. The red line shows the median and the red crosses show the outliers of the data.

Estimating capacity from RLS and WLS. Table 4.4 and Figures 4.25 and 4.26 show the results from the capacity estimates using WLS and RLS. The variables x_i are taken from the SoC from the EKF from the model with only one state in the EKF. The variables y_i are taken from the current from the EKF from the model with only one state in the EKF. The variables x_i and y_i are taken when the SoC changes with 0.5%.

Table 4.4 The results from an estimated capacity and SoH from different amounts of cycles made on one battery cell. The table shows the results of the estimated capacity using WLS and RLS.

Cycles	Q_c (Ah)	Q_{wls} (Ah)	SoH_c (%)	SoH_{wls} (%)
84	109.35	109.38	102.20	102.22
100	110.78	110.34	103.53	103.13
120	109.86	109.98	102.67	102.79
124	109.24	109.61	102.09	102.44
156	110.26	110.18	103.05	102.97
172	108.33	108.45	101.24	101.35
180	116.06	110.04	108.47	102.84
184	112.30	111.86	104.95	104.54
200	111.31	110.09	104.03	102.86

The current for the 84th and the 120th cycles was around 32A, while the current for the rest was around 37.5A.

In Table 4.4, Q_c is the estimated total capacity in Ah using equation (3.46) where c_1 and c_2 are determined as described in Chapter 3. Q_{wls} is the capacity calculated using weighted least squares. SoH_c is the SoH using Q_c and SoH_{wls} is the SoH using Q_{wls}. The WLS and the RLS are only computed for a charging cell. The nominal capacity used to calculate SoH is 107Ah.

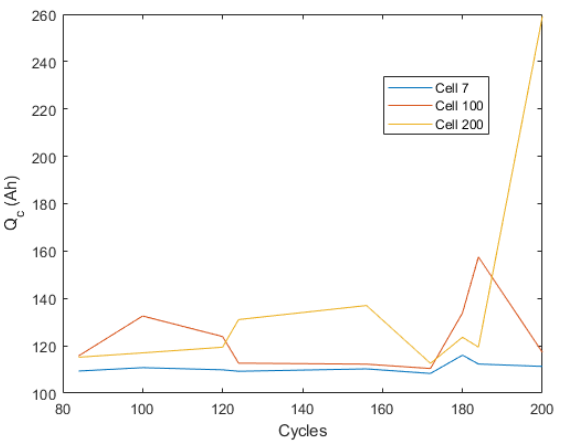

Figure 4.25 Estimated capacity Q_c from RLS for one cell for three different cells.

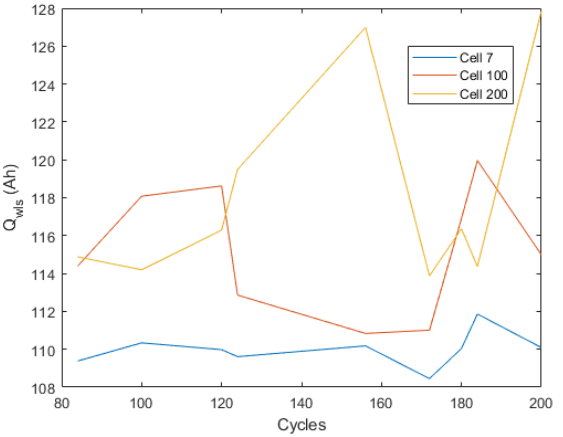

Figure 4.26 Estimated Capacity Q_{wls} from WLS for one cell for three different cells.

Figure 4.25 present the results of the estimated capacity from a different number of cycles performed on the battery using RLS. Figure 4.26 presents the estimated capacity results from a different number of cycles performed on the battery using WLS. The results of both RLS and WLS behave stochastically and seem to have large errors. Cell 7 for both RLS and WLS seems to have provided the most reliable and stable results out of the three cells presented.

Validating the model. The validation was carried out by calculating the R^2 of the WLS. Then, the Residual sum of squares (RSS) was calculated using equation (3.50). The total sum of squares (TSS) was calculated using equation (3.49). The R^2 was calculated using equation (3.48) and the RSS and TSS results. The standard deviation of the residual (σ_R) was calculated using equation (3.51). The results are presented in Table 4.5.

Table 4.5 Results used to validate WLS

TSS	20667
RSS	34.2966
R^2	0.9983
Q_{ch}	0.0017
σ_R	0.5916

5

Discussion

This chapter will discuss the results and what they might imply. First, the estimation of R_0 appeared unreliable, so the original values for R_0 were used. The model was updated to do capacity estimation and follow V_{term} as well as possible. The estimation results will be discussed. Lastly, the challenges with the entire project are discussed.

Estimating the equivalent series resistance. As seen in Chapter 4, estimating the equivalent series resistance (R_0) proved challenging. The BMS controls the battery cells and engages or bypasses them. The number of measurements that can be taken is limited by the BMS. Since the change in current needs to be significant, the measurements can only be taken when the battery cell is engaged or bypassed. The more recorded measurements, the more accurate our estimation will be. The results of the estimated R_0 presented in Figure 4.3 do not show any clear sign of degradation. As mentioned in [Xiong and Shen, n.d.], the battery is considered at its EoL when the R_0 has doubled. An increase in R_0 might indicate that the R_0 might increase as the battery ages. However, an increase in R_0 is not visible in Figure 4.3. The partial reason why this is not visible might be that the number of cycles tested (200 cycles, which is at its EoL after 2000 cycles) is not large enough for a change in R_0 to be observed. Another partial reason is that the estimations of R_0 have a considerable error. The filtered results of R_0 as shown in Table 4.1 and the nominal R_0 of the battery is at $0.7\text{m}\Omega$, and if it is considered at its EoL when R_0 has doubled, then the EoL is when $R_0 = 1.4\text{m}\Omega$. In Table 4.1, R_0 is not only too high but R_0 increases and decreases with the increase in cycles run. A possibility is that R_0 has not changed significantly for a change to be observed and that the measurements are wrong. The uncertainty in the estimation of R_0 resulted in the estimation of R_0 not being used in the thesis, but an approximation of how R_0 would change with the degradation was used in the degrading model. The estimate of R_0 is wrong because R_0 is too high compared to the estimated useful capacity of the battery. During the charge and discharge, R_0 changes with SoC and temperature. In order to perform a more accurate estimation of R_0, the SoC and temperature would have to be included, along with more cell switching, to get more data to determine R_0.

2-RC model with an EKF

As shown in Figures 4.5 and 4.6, the model for when the battery is charging follows the measured results much better than the discharging plot. The difference between the battery charging results could be that the values for R_0, R_1, R_2, C_1, and C_2 are closer to the actual values for when the battery is charging than discharging. The difference between the charging and the discharging results could also be due to the different efficiency of charging and discharging the battery. It could also be that degradation is more visible when the battery discharges than for charging. The difference between the model and the actual results is signs of degradation. This assumption can only be made if the model is perfect. The model does not consider degradation. The EKF considers the model's measurements and results and attempts to estimate the correct state values. The terminal voltage (V_{term}) from the EKF in Figure 4.5 is not very noisy, but the V_{term} from the EKF in Figure 4.6 is very noisy. The reason for the noise is that the value for the measurement covariance is smaller for the discharging EKF than for the charging EKF. Smaller measurement noise covariance makes the EKF trust the measurements more for discharging than charging and attempts to follow the measurements more. However, since the model has a significant error for discharging, the EKF becomes worse at filtering the noise.

The only method to know the SoC of this model is Coulomb counting. Only estimating the SoC from Coulomb counting limits the capacity estimation techniques that can be used for this mode. The only way of estimating the capacity was by Coulomb counting or Watt counting.

Model with SoC as a state

The third state in the model was introduced to estimate the SoC in ways other than Coulomb counting. When the SoC was added as a state, it allowed the EKF to estimate the SoC. The model is a bit off with the third state; the models V_{term} has a more significant error in the start of charge and a similar error in discharge with three states in Figures 4.7 and 4.8 compared to the model with two states in Figures 4.5 and 4.6. For discharging, the EKF is in between the model and the measurements, which is desired. From Figures 4.7 and 4.8, it seems like the discharging model is better than the charging model. However, with the SoC, as shown in Figures 4.9 and 4.10, the charging model follows the measurements better than the discharging. Therefore, the SoC for discharging is a clear error in the model, and the EKF's SoC should not be negative. A possible reason for the significant error is that the discharging model has a smaller measurement noise covariance than the charging. The smaller measurement noise covariance allows the V_{term} from the EKF to follow the measurements of V_{term} closer but also picks up some of the noise from the measurements. The EKF deviates from the model, which might be why the SoC state in the EKF deviates from the Coulomb-counted SoC. The reason for this error could be that the EKF attempts to correct the values of the voltage with the values of the SoC and finds correlations between them that do not exist. The significant error makes

the EKF compensate for the error more that it changes the SoC so drastically that it becomes negative. Since the SoC becomes negative, it indicates something is wrong with the model.

Model of 2-RC and SoC as the only state in the EKF

The 2-RC model and SoC as the only state in the EKF can follow the measuments better than when the EKF had three states, especially for SoC as seen in Figure 4.10 compared to Figure 4.8. This model is more simplistic since it only has one state and might make it easier for the EKF to estimate the state with less error. The model of 2-RC and SoC as the only state in the EKF has a higher measurement noise covariance, allowing it to trust the model more and the measurements less. The higher measurement noise covariance might be one reason why this model follows the Coulomb counted SOC better than the model with three states in the EKF. This model and EKF V_{term} follow the measurements of V_{term} well for charging, and the EKF V_{term} follows the model V_{term} well for discharging, but the model and EKF has a more significant error to the measurements of V_{term} for discharging. The error might be primarily due to the model being slightly off for discharging compared to charging. The V_{oc} affects the model to a large extent, so V_{oc} might be prone to a more significant error for discharging than charging. The V_{oc} was used from previous data [Pinter et al., n.d.], and the V_{oc} might need to be redone for discharging the cell. The SoC estimated with the EKF followed the Coulumb counted SoC better as seen in Figures 4.15 and 4.16 than the model with three states and three states in the EKF as seen in Figures 4.9 and 4.10. However, it has a more significant error for discharging, which might be due to the model being more off than discharging. The EKF has problems handling when the cell is suddenly switched off, and the SoC is not supposed to change. This error might be due to V_{term} still changing even when no current exists. The EKF filters the signal well and can handle switching the cell off and the constant error due to not having a perfect model. The switching of the cell can be seen in Figures 4.13 and 4.14 when V_{term} suddenly increases or decreases or in Figures 4.15 and 4.16 when the SoC does not increase or decrease. The error between the SoC from the model and the EKF and the error between the measured V_{term} and the modeled and EKF V_{term} might be due to changes in the capacity that might indicate changes in SoH, but it could also be due to modeling errors.

Degrading model

The degrading model has made some significant assumptions about how the battery degrades. However, validating the accuracy of the degrading model is complex and would require either opening up the battery or fully degrading the battery [Xiong and Shen, n.d.].

From the simulation, the battery has degraded by around 8% after 200 cycles. The degradation rate implies that after 2000 cycles, it will have degraded 80% since the assumption is made that it will degrade linearly until 2000 cycles. How the bat-

tery will degrade after 2000 cycles is entirely unknown to the author. A specific test on the cell where it is degraded past 2000 cycles would be necessary to determine how the battery degrades after 2000 cycles.

The capacity was calculated in Ah and Wh for the data received from the degrading model for 1, 100, and 200 cycles. The results in Table 4.2 shows how the useful capacity slowly decreases as the number of cycles increases, as expected. The results of the SoH in Table 4.3 also show how the SoH decreases with the number of cycles as expected. Just because this is what the degrading model illustrates does not mean that this is how the battery will behave in reality.

The degrading model gave a nominal capacity $Q_{nom,Wh}$ for charging and discharging and a useful nominal capacity $Q_{u,nom,Wh}$ for charging and discharging. Since the technical specification did not specify a capacity in Wh, this result seems more realistic than using the lower or higher operational voltage to estimate a large span for the nominal capacity in Wh.

The degrading model does not switch on and off the cells during charge and discharge as the BMS does in the actual charging and discharging of the battery. Switching the cell on and off does not affect the voltage during operations, but how it affects degradation is unknown to the author.

SoH estimation

Estimating the SoH using the battery's capacity in Wh proved difficult since the nominal capacity in Wh of the battery is not given by the supplier of the battery. What exists is the capacity in Ah, which is 100Ah, and the operational voltage range, which is between 2.8V and 3.8V. Since the tests are performed at a lower C-rate (around C/3), the nominal capacity increases to around 107Ah, the operational voltage, however, is the same. However, with the voltage ranges, the battery's energy can be either 299.6Wh or 406.6Wh, which is a considerable range. From the degrading model, a nominal capacity in Wh was acquired to be $Q_{nom,Wh} = 356.63$Wh for charging and $Q_{nom,Wh} = 352.19$Wh for discharging. This nominal capacity seems more reasonable because it implies a V_{term} of around 3.3V, in the middle of the operating voltage range. Therefore, the $Q_{nom,Wh}$ from the degrading model has been used to determine the SoH from the capacity in Wh.

SoH estimation from Coulomb and Watt counting. Estimating the capacity from Coulomb counting proved challenging for determining whether capacity and the SoH have changed. From Figures 4.19 and 4.20, it can be observed that the useful capacity is very different for all 297 cells. The difference in useful capacity might be due to the cells being at different levels of SoH or that the BMS prioritized some cells more than others. The difference in useful capacity might also be that the cells were differently degraded when inserted in the whole battery system. From Figure 4.19, the cell's capacity can be classified into three different regions for charging, one large region with a capacity of 67Ah, another smaller one with almost 75Ah, and a third with above 90Ah for 84 to 100 cycles. For 200 cycles,

there seems to be one region around 70Ah, one smaller around 77Ah, and a small above 90Ah. From Figure 4.20 for discharging then, there seem to be two clusters, one with a capacity of around 68 Ah and another around 78Ah for all cycles. However, between 68Ah and 78Ah are more spread out than for the charging. The more extensive spread for discharging and the more apparent regions for charging might explain why the charging box plots in Figures 4.21 and 4.23 have outliers while the discharging box plots in Figure 4.22 and 4.24 do not have any outliers. Why this region occurs is unknown to the author. It could have to do with the balancing algorithm of the BMS or the cells being degraded and performed differently.

Any change in the useful capacity in Ah or Wh is challenging to observe from the Figures 4.21, 4.22, 4.23 and 4.23 that illustrate the estimated useful capacity. Any change in useful capacity is difficult to observe because the useful capacity fluctuates, increases, and decreases sporadically with the number of cycles. The sporadic change in capacity makes it difficult to determine whether the capacity changes because of degradation or if the capacity changes due to the BMS. For example, there seem to be signs of degradation for the discharging cells until 184 cycles, and then the capacity increased. The capacity of a battery is known to increase if it has been resting for a long time and then is used extensively again, but the lack of knowledge of how the BMS works makes it challenging to determine if this is the case.

For the SoH to be calculated, the useful capacity is divided by the nominal useful capacity. The nominal useful capacity is 85.6Ah for charging and discharging, and it was estimated to be 289.1Wh for charging and 281.75Wh for discharging. The SoH is more than 100% for some cells and less than 80% for others. Both an SoH over 100% and less than 80% are unreasonable. Since the capacity fluctuates with the number of cycles and the spread is so large, no conclusion can be drawn from the current SoH or the change of SoH with this method and the number of cycles performed.

SoH estimation from WLS and RLS. The capacity was estimated from the results acquired from the model with two states and one state in the EKF, the SoC. Table 4.4 and Figures 4.25 and 4.26 illustrate the results of the capacity estimation using WLS and RLS. From Figures 4.25 and 4.26, the capacity seems not to change significantly with more cycles performed, except after 180 cycles, then the capacity seems to increase. The expectation is that the capacity will decrease with more cycles run on the battery. However, the capacity increase after 180 cycles when considering cell 200 in Figure 4.25 would indicate a capacity increase of almost 160%. The high capacity is unreasonable and indicates an error in the capacity estimation. Cell 7 in Figures 4.25 and 4.26 does not change significantly and is around 110 Ah. The capacity fluctuates slightly but does not seem to decrease. If the capacity estimations for cell 7 in Figures 4.25 and 4.26 are correct, the state of health would be slightly larger than 100%. An SoH larger than 100% would indicate that the estimation of the nominal capacity of 107Ah has a small error and that the nominal capacity is

larger than 107Ah.

The testing stayed more or less the same for all cycles, charged and discharged at around 37.5A, except for cycles 84 and 120. After that, it was charged and discharged at 32A. As mentioned earlier, discharging at a lower C-rate should increase the battery's capacity. However, this is not the case from the results in Figures 4.25 and 4.26. Therefore, with fewer cycles and a lower C-rate, the battery's capacity is expected to be higher than with a higher C-rate and more cycles performed.

The WLS assumes measurement noise on y_i but not on x_i. If there is more measurement noise on x_i than y_i, then the values for x_i and y_i could be switched. The new $y_i = x_i$ and new $x_i = y_i$. Changing x_i and y_i could give different results, especially if there is more measurement noise on x_i than y_i.

Validating the model. The validation was done using the R^2 to determine the model's goodness of fit. As seen in the results, the value of R^2 is high, and 1-R^2 is larger than 0.001. Therefore, the results for R^2 indicated that the model was acceptable. However, the values for the capacity estimation are off for some of the cells, such as cell 200, after 200 cycles. The standard deviation of the residual (σ_R) was calculated to be 0.5916, which is small for the residual values and indicates that the error is relatively small. Therefore, the method to estimate the capacity using WLS and RLS might be accurate, but the values received for SoC might need to be revised. Figures 4.13 and 4.14 show that the model deviates from the actual measurements. The model shows a higher V_{term} than the measurements and might explain why the capacity is larger than the nominal for the estimation. With a more accurate model, capacity estimations should be more accurate.

Limitation of the EKF. The EKF results depend on the measurement noise covariance, process noise covariance, and output y. The smaller the process noise covariance is, the more trust in the model. The smaller the measurement noise covariance is, the more trust in the measurements. The accuracy of the EKF correlates with the model's accuracy. Since there is an almost constant error between the model and the measurements, the model is imperfect. The imperfect model limits the accuracy of the EKF since it depends on the model. The process noise covariance can be made more prominent and the measurement noise covariance smaller. Still, the state estimation attempts to compensate for the error, and the state estimations can no longer be trusted. This phenomenon is known as filter divergence and can be seen in Figure 4.10 that illustrates the SoC for discharging for the model with three states where SoC is one state [Robert Grover Brown, 2012].

Summary

The battery model is a phenomenological model of the battery. It is difficult to capture all the battery dynamics, so the model is an approximation. The model behaves well and follows the process well for charging the battery. As the SoH change, the model's parameters are expected to change. The model's parameters could be updated continuously with changes in SoH. However, this requires specific tests and

is very tedious. Instead, the change in parameters could be used to determine the SoH, and the validation for this would be that the model follows the measurements perfectly.

The significant error when discharging the battery could be due to multiple factors. The error between discharging and charging could imply that as the battery ages, the performance of the battery when it charges and discharges deviates independently of each other. The parameters used in the model could also be different when charging and discharging the battery. The V_{oc} was assumed not to change when creating the model. The V_{oc} significantly influences the model's performance and can lead to huge errors. The V_{oc} was acquired through previous data. To gather results for the V_{oc} changes with degradation, then specific charging and discharging test would have to be performed. These tests would be extremely time-consuming as the battery would have to be stopped during charge and discharge until a steady state is reached to record the V_{oc}.

The estimator that was used to estimate the correct parameters was an EKF. From the results, the noise is Gaussian noise, where a Kalman filter is the optimal observer for a linear model. The process is, however, non-linear, so an EKF was applied to handle the non-linear system [Zucconi, n.d.]. Since the Kalman filter can be used for smoothing and estimating, it is an excellent option. The EKF worked well for filtering the data, but the model had errors that caused the EKF to deviate. The EKF works well when the model is known. However, since the model is not well known, the EKF will not work well. The initial guess did not significantly influence the result, but the estimation error greatly affected the results. Therefore, the EKF also needs to perform some iterations to create and achieve high accuracy. However, this is fine since charging and discharging a battery is slow. The most significant problem with using the EKF is the model's accuracy. The less accuracy of the model, the lower the estimation accuracy will be.

Challenges

From the state-of-the-art review, it is apparent that there is no unified definition of SoH. The difference in SoH makes it challenging to know how well an acquired battery will perform and for how long and when acquiring a battery. The technical specification does not clarify what the supplier has used for EoL. However, when considering batteries, the EoL of most batteries is when the capacity has dropped 80% compared to the nominal. Not knowing when the battery is considered at its EoL makes it challenging to predict the total lifetime of the battery.

The battery that has been used consists of LFP battery cells. The $V_{oc} - SoC$ curve is exceptionally flat for LFP cells. The flat $V_{oc} - SoC$, along with the slow parameter changes, makes it difficult to use a dynamic filter such as the EKF [Tran et al., 2021].

The battery system could be better known. The cells that make up the battery system have little to previous knowledge of the cells. Where the cells originally

come from and how much they have been used is unknown. Little previous knowledge of the cells made it difficult to create an accurate model of a degrading battery since the performance of a nominal battery cell is missing. The tests that could be performed needed to be more comprehensive to accurately estimate some parameters of the model, such as the open circuit voltage.

The cell's current rapidly increases at the start of a charge or a discharge. The rapid increase in current might have been a cause for some of the fuses in the inverter/rectifier to break. The breaking of the fuses made it impossible to charge and discharge the battery, and testing stopped for a couple of days until the fuse was fixed. In addition, there was a problem with controlling the battery. The VPN connection was lost and did not work just to restart the entire system. The solution to the problem was to switch the router on the battery system, and then the problem with the VPN connection no longer occurred, and testing could proceed as usual. The cause of the problem might have been due to the router breaking or the sim card in the router breaking or overusing data. However, stopping the tests limited the possibility of doing enough tests to see a degradation of the battery's cells.

6

Conclusion

This chapter will summarize and conclude the thesis. The chapter will start by concluding the estimation and definition of SoH. Then the challenges with the modeling and capacity estimation will be explained. Finally, this chapter will conclude by explaining what improvements are viable.

The complexity of the lithium iron phosphate battery and the need for prior knowledge of the battery made it challenging to determine the SoH of the battery system. Furthermore, validating the results of the SoH is very challenging. To the author, there is no known way of validating exactly how much the battery will degrade or how much the battery has degraded without prior knowledge of the battery with the method used in this thesis and the testing equipment. Prior knowledge of the battery system at its beginning of life is vital for accurately determining the SoH of the battery with the method used.

There is no unified definition for determining the SoH or a definition for SoH in literature. The most common way of defining SoH in literature is from capacity fade or increase in R_0. Most methods used to determine SoH use specific and controlled testing environments, such as with only one cell and in a temperature chamber. By deviating from these methods, SoH became hard to determine from both using the change in useful capacity compared to the nominal, comparing the change in total capacity compared to the nominal, and from changes in the equivalent series resistance compared to the nominal.

The idea at the start of the thesis was to compare the battery's useful capacity to the battery's nominal useful capacity. However, since the BMS balancing algorithm switches on and off the cells unpredictably, the estimated useful capacity of the cells became unreliable, so the SoH estimation became unreliable. Instead, the method of using WLS and RLS seemed more promising. However, this was also unsuccessful, with a lack of knowledge of the nominal capacity and no significant change observed in the capacity. The inaccuracy of the capacity estimation using WLS and RLS are largely due to the model's inaccuracy. A model with higher accuracy would allow for a more accurate capacity estimate. Other models with an unscented Kalman filter or dual estimation techniques might give better results, as discussed by Greggory Plett [Plett, 2015].

Deriving a model of the battery was challenging but seemed promising. It was an iterative process where the models were adjusted and changed to optimize them. The result is a model that could follow the terminal voltage and estimate the SoC. More testing on the model would be necessary to validate the model.

The results that could be obtained are a very rough estimate of the SoH of the battery, and no change can be seen with confidence. The low change in SoH limits the ability to predict degradation, and the only model to predict degradation is the degrading model. It can be used to guess how much the battery has degraded and predict how much more it can be used. However, the degrading model did not correlate with the test results, which might be because large assumptions have been made on how the battery would degrade in the degrading model. Changes in the C-rate will affect the battery unpredictably. From the literature, a C-rate should result in a lower capacity. However, this conclusion can not be drawn from the acquired results.

Using the WLS and RLS methods, the current capacity might have been determined for some of the cells but had a significant error in some cells. Even if WLS or RLS is an efficient way of estimating the capacity, the SoH can only be determined if the nominal capacity is known. It can, however, be used to see changes in capacity but not to determine SoH if not the nominal capacity is known.

Future work

A difficulty in creating the battery model is the lack of previous knowledge. What could have been done is to take one cell from the entire battery system and perform extensive testing on one cell to find the initial parameters to see how one cell degrades by itself. The complexity that comes with 297 cells and a BMS that controls the performance of the cells makes it difficult to know if it is that cell that has degraded or the BMS that has switched the cell off for whatever reason. With knowledge of how one cell behaves as it is degraded, it would be easier to scale up and apply it to the entire system. A more robust mathematical algorithm could be implemented and tested instead of WLS and RLS. A more robust algorithm might lead to more likely results for capacity estimation.

The battery could be tested more. More testing might cause a significant change in capacity. A significant change in capacity would allow for changes in SoH to be detected. More testing also creates more data that could be used to increase the accuracy of the estimation of SoH. More data also allows for other methods for SoH estimation, such as implementing ML in DD-driven methods that require large amounts of data.

The data processing took a long time. The vast amount of data became too much to handle. The battery has been discharged for 200 cycles; one cycle implies one discharge and one charge. One cycle takes around 5 hours to complete. There are 297 cells, and each cell's measurements are taken every second on the temperature, current, SoC, voltage, and engagement. A more efficient way of handling the data

would make this project easier and more information could be extracted from the data.

Other tests could be implemented, such as simulating the effect that the grid and charging of EV would have on the SoH of the battery. The effect on the battery could also be implemented if used for frequency control. For example, the fast responses needed for the battery can create large currents that might affect the SoH of the battery. This testing would require a specific test that would take a very long time. To perform these tests, the model for estimating the SoH would need to be validated.

Bibliography

ApS, N. S. S. (n.d.). *Topcharge - variable topology battery system for optimising grid load during high-power charging of electric vehicles*. URL: https://energiforskning.dk/en/node/15893. (accessed: 31.10.2022).

Automatic Control LTH, D. of (n.d.). *Automatic control - Advanced course*. URL: https://www.control.lth.se/education/engineering-program/frtn55-automatic-control-advanced-course/. (accessed: 04.11.2022).

B.S. Everitt, A. S. (2010). *The Cambridge Dictionary of Statistics 4th Edition*. Cambridge.

Birkl, C. R., M. R. Roberts, E. McTurk, P. G. Bruce, and D. A. Howey (2017). "Degradation diagnostics for lithium ion cells". *Journal of Power Sources* **341**, pp. 373–386. ISSN: 03787753. DOI: 10.1016/j.jpowsour.2016.12.011.

Bloch, C., J. Newcomb, S. Shiledar, and M. Tyson (n.d.). *BREAKTHROUGH BATTERIES Powering the Era of Clean Electrification*. URL: http://www.rmi.org/breakthrough-batteries.

Calearo, L., C. Ziras, A. Thingvad, and M. Marinelli (2022). "Agnostic battery management system capacity estimation for electric vehicles". *Energies* **15** (24), p. 9656. ISSN: 1996-1073. DOI: 10.3390/en15249656. URL: https://www.mdpi.com/1996-1073/15/24/9656.

Cârstoiu, G., M. V. Micea, L. Ungurean, and M. Marcu (2021). "Novel battery wear leveling method for large-scale reconfigurable battery packs". *International Journal of Energy Research* **45** (2), pp. 1932–1947. ISSN: 1099114X. DOI: 10.1002/er.5879.

Clevert, D. A., T. Unterthiner, and S. Hochreiter (2016). "Fast and accurate deep network learning by exponential linear units (ELU)". In: International Conference on Learning Representations, ICLR.

Couto, L. D., J. Schorsch, N. Job, A. Léonard, and M. Kinnaert (2019). "State of health estimation for lithium ion batteries based on an equivalent-hydraulic model: an iron phosphate application". *Journal of Energy Storage* **21**, pp. 259–271. ISSN: 2352152X. DOI: 10.1016/j.est.2018.11.001.

Couto, L. D., M. Charkhgard, B. Karaman, N. Job, and M. Kinnaert (2022). "Lithium-ion battery design optimization based on a dimensionless reduced-order electrochemical model". *Energy*, p. 125966. ISSN: 03605442. DOI: 10.1016/j.energy.2022.125966.

Coverdan (n.d.). URL: https://www.converdan.com/. (accessed: 15.02.2023).

El-Dalahmeh, M., J. Lillystone, M. Al-Greer, and M. El-Dalahmeh (2021). "State of health estimation of lithium-ion batteries based on data-driven techniques". In: *2021 56th International Universities Power Engineering Conference (UPEC)*. DOI: 10.1109/UPEC50034.2021.9548209.

Denholm, P., T. Mai, R. W. Kenyon, B. Kroposki, and M. O'malley (2020). *Inertia and the Power Grid: A Guide Without the Spin*. URL: www.nrel.gov/publications. (accessed: 04.11.2022).

entsoe (n.d.). *Inertia and rate of change of frequency (rocof)*. URL: https://eepublicdownloads.azureedge.net/clean-documents/SOC20documents/Inertia20and20RoCoF_v17_clean.pdf. (accessed: 15.02.2023).

Eurostat (n.d.). *Electricity prices for household consumers*. URL: https://ec.europa.eu/eurostat/databrowser/view/NRG_PC_204__custom_4905840/settings_2/table?lang=en. (accessed: 10.02.2023).

Foundation, O. (n.d.). *What is OPC?* URL: https://opcfoundation.org/about/what-is-opc/. (accessed: 05.12.2022).

Glad, T. and L. Ljung (2000). *Control Theory*. Multivariable and Nonlinear Control. CRC Press. ISBN: 0-7484-0878-9.

Hamada, H., Y. Kusayanagi, M. Tatematsu, M. Watanabe, and H. Kikusato (2022). "Challenges for a reduced inertia power system due to the large-scale integration of renewable energy". *Global Energy Interconnection* **5** (3), pp. 266–273. ISSN: 25900358. DOI: 10.1016/j.gloei.2022.06.003.

Jenu, S., A. Hentunen, J. Haavisto, and M. Pihlatie (2022). "State of health estimation of cycle aged large format lithium-ion cells based on partial charging". *Journal of Energy Storage* **46**. ISSN: 2352152X. DOI: 10.1016/j.est.2021.103855.

Kong, X. R., A. Bonakdarpour, B. T. Wetton, D. P. Wilkinson, and B. Gopaluni (2018). "State of health estimation for lithium-ion batteries". In: Elsevier B.V., pp. 667–671. DOI: 10.1016/j.ifacol.2018.09.347.

Kundur, P. (1994). *Power systems stability and control*. McGraw-Hill Irwin.

Kutner, M., C. Nachtsheim, J. Neter, and W. Li (2005). *Applied Linear Statistical Models*. McGraw-Hill Irwin.

MathWorks (n.d.). *Math. graphics. programming.* URL: https://se.mathworks.com/products/matlab.html. (accessed: 15.02.2023).

Moreno, A. B. (2021). *Machine Learning-based Online State-of-Health Estimation of Electric Vehicle Batteries Artificial Intelligence Applied to Battery Management Systems [Master's Thesis, Aalborg University]*. URL: http://www.aau.dk.

Nerve (n.d.). *EV high power charge anywhere*. URL: https://nervesmartsystems.com/. (accessed: 15.02.2023).

OleumTech (n.d.). *What is scada? supervisory control and data acquisition*. URL: https://oleumtech.com/what-is-scada#:~:text=SCADA. (accessed: 15.02.2023).

Pates, R. and E. Mallada (2018). "Robust scale-free synthesis for frequency control in power systems". URL: http://arxiv.org/abs/1804.00729.

Pinter, Z. M., J. Engelhardt, G. Rohde, C. Traeholt, and M. Marinelli (n.d.). *Validation of a Single-Cell Reference Model for the Control of a Reconfigurable Battery System*. ISBN: 9781665409711. URL: http://topcharge.eu/.

Pinter, Z. M., D. Papageorgiou, G. Rohde, M. Marinelli, and C. Træholt (2021). "Review of control algorithms for reconfigurable battery systems with an industrial example". In: *2021 56th International Universities Power Engineering Conference (UPEC)*. DOI: 10.1109/UPEC50034.2021.9548259.

Plett, G. (2015). *Battery Management Systems, Volume II: Equivalent-Circuit Methods*. Artech House Publishers. ISBN: 9781630810276.

PowerLabDK (n.d.). *Organisation*. URL: https://www.powerlab.dk/about_powerlabdk/organisation. (accessed: 10.12.2022).

Robert Grover Brown, P. Y. C. H. (2012). *Introduction to Random Signals and Applied Kalman Filtering*. John Wiley Sons, Inc.

Sandberg, K.-O. (2016). *Kartläggning av frekvensreglering i det nordiska synkrona kraftsystemet Ny strategi för balansregleringar från driftplaner?* URL: http://www.teknat.uu.se/student. (accessed: 31.10.2022).

Schmidt, S., P. Andreas, and T. Valgreen (n.d.). *Performance Characterisation and Dynamical Behaviour of a Reconfigurable Battery System*. URL: www.elektro.dtu.dk/cee. accessed: 31.10.2022.

Sinopoly battery systems (n.d.). URL: http://www.sinopolybattery.com/en/products.aspx?cid=10. (accessed: 15.02.2023).

Strutz, T. (2016). *Data Fitting and Uncertainty*. Springer.

Tatham, S. (n.d.). *Putty: a free ssh and telnet client*. URL: https://www.chiark.greenend.org.uk/~sgtatham/putty/. (accessed: 05.12.2022).

Thingvad, A., L. Calearo, P. B. Andersen, and M. Marinelli (2021). "Empirical capacity measurements of electric vehicles subject to battery degradation from V2G services". *IEEE Transactions on Vehicular Technology* **70** (8), pp. 7547–7557. ISSN: 19399359. DOI: 10.1109/TVT.2021.3093161.

Thingvad, M., L. Calearo, A. Thingvad, R. Viskinde, and M. Marinelli (2020). "Characterization of NMC lithium-ion battery degradation for improved online state estimation". In: *2020 55th International Universities Power Engineering Conference (UPEC)*. DOI: 10.1109/UPEC49904.2020.9209879.

Trafikanalys (n.d.). *Eldrivna vägfordon-ägande*. URL: www.trafa.se. accessed: 31.10.2022.

Tran, M.-K., A. Dacosta, A. Mevawalla, S. Panchal, and M. Fowler (2021). "Comparative study of equivalent circuit models performance in four common lithium-ion batteries: LFP, NMC, LMO, NCA". *Batteries* **7**. DOI: 10.3390/batteries7030051.

UN (n.d.). *The climate crisis a race we can win*. URL: https://www.un.org/en/un75/climate-crisis-race-we-can-win. (accessed: 15.02.2023).

Wang, L., J. Qiu, X. Wang, L. Chen, G. Cao, J. Wang, H. Zhang, and X. He (2022). "Insights for understanding multiscale degradation of lifepo4 cathodes". *eScience* **2** (2), pp. 125–137. ISSN: 26671417. DOI: 10.1016/j.esci.2022.03.006.

Wu, B., W. D. Widanage, S. Yang, and X. Liu (2020). "Battery digital twins: perspectives on the fusion of models, data and artificial intelligence for smart battery management systems". *Energy and AI* **1**. ISSN: 26665468. DOI: 10.1016/j.egyai.2020.100016.

Xing, W., H. Wang, L. Lu, X. Han, K. Sun, and M. Ouyang (2021). "An adaptive virtual inertia control strategy for distributed battery energy storage system in microgrids". *Energy* **233**. ISSN: 03605442. DOI: 10.1016/j.energy.2021.121155.

Xiong, R. (n.d.). *Battery Management Algorithm for Electric Vehicles*. Springer. ISBN: 978-7-111-60864-6.

Xiong, R. and W. Shen (n.d.). *Advanced battery management technologies for electric vehicles*. Wiley. ISBN: 9781119481676.

Yang, S., C. Zhang, J. Jiang, W. Zhang, L. Zhang, and Y. Wang (2021). *Review on state-of-health of lithium-ion batteries: Characterizations, estimations and applications*. DOI: 10.1016/j.jclepro.2021.128015.

Zhou, Y., M. Huang, and M. Pecht (2018). "An online state of health estimation method for lithium-ion batteries based on integrated voltage". In: 2018 IEEE International Conference on Prognostics and Health Management (ICPHM). ISBN: 9781538611647. DOI: 10.1109/ICPHM.2018.8448947.

Zucconi, A. (n.d.). *The extended Kalman filter*. URL: https://www.alanzucconi.com/2022/07/24/extended-kalman-filter/. (accessed: 15.02.2023).

Lund University
Department of Automatic Control
Box 118
SE-221 00 Lund Sweden

Document name
MASTER'S THESIS

Date of issue
June 2023

Document Number
TFRT-6214

Author(s)
Carl Spångberg

Supervisor
Zoltan Mark Pinter, DTU, Denmark
Dimitrios Papageorgiou, , DTU, Denmark
Chunyang Zhao, , DTU, Denmark
Richard Pates, Dept. of Automatic Control, Lund University, Sweden
Björn Olofsson, Dept. of Automatic Control, Lund University, Sweden (examiner)

Title and subtitle
State of Health estimation of battery systems

Abstract

This study focuses on estimating the state of health (SoH) of a lithium iron phosphate (LFP) battery system, which is crucial for assessing the value and lifespan of new or used batteries in energy storage, grid support, and electric vehicle applications. A proposed method for determining SoH based on comparing useful and nominal useful capacities in Ah and Wh, as well as total and nominal capacity, has been presented. To validate the method, 200 charging and discharging cycles over five months were performed. Three models were developed to track battery behavior and one model to simulate degradation. An extended Kalman filter has been used in the model to estimate the battery's non-linear parameters and filter the noisy measurements. The models revealed that while estimating capacity using Coulomb and Watt counting proved difficult for the battery system that has been used, weighted least squares and recursive weighted least squares methods showed promise for determining current capacity. Furthermore, an attempt to estimate the battery's equivalent series resistance was performed, but no conclusion could be drawn due to limited knowledge of battery parameters. The findings highlight the challenges of modeling and estimating the SoH of used batteries and suggest the need for more targeted experimentation to improve battery modeling and estimation accuracy.

Keywords

Classification system and/or index terms (if any)

Supplementary bibliographical information

ISSN and key title
0280-5316

ISBN

Language
English

Number of pages
1-86

Recipient's notes

Security classification